# Microarray Analysis of Nonfunctional Ribosomal RNA Decay in *Saccharomyces cerevisiae*

Kathryn Elizabeth Driest
Defended on April 28, 2014
Washington and Lee University
Department of Chemistry and Biochemistry

In fulfillment of Honors in Biochemistry

**Table of Contents**

Abstract.....5

Introduction.....6-25

Methods and Materials.....26-42

Results and Discussion.....43-66

Conclusion.....67-68

Appendix.....69-78

References.....79-81

**List of Tables**

Table 1: Yeast strains used in this study....26
Table 2: Plasmids used in this study....28
Table 3: Primer sets used for RT-qPCR analysis....35
Table 4: RT-qPCR analysis of BY4741 transformants....45
Table 5: RT-qPCR analysis of NOY504 transformed with pSC1 plasmids....47
Table 6: RT-qPCR analysis of NOY504 transformed with pWL160 and pSC1 plasmids....47
Table 7: RT-qPCR analysis of NOY504 transformed with pWL155 and pSC1 plasmids....48
Table 8: Partial list of differentially expressed genes identified by microarray analysis of mutant 18S and 25S transformants....59
Table 9: Partial list of differentially expressed genes identified by microarray analysis of double-mutant transformant....66
Table 10: Partial list of differentially expressed genes identified by DEDS....78

**List of Figures**

Figure 1: Structure of the eukaryotic ribosome at 3.0 Å resolution....7
Figure 2: Processing of pre-rRNA in *Saccharomyces cerevisiae*....9
Figure 3: Overview of the ribosome synthesis pathway....11
Figure 4: Mechanism of translation initiation in eukaryotes....14
Figure 5: Mechanism of translation elongation in eukaryotes....16
Figure 6: Mechanism of translation termination in eukaryotes....16
Figure 7: Models for 18S NRD and 25S NRD....20
Figure 8: Expression ratios for normal WT/18S microarray and WT/25S microarray....23
Figure 9: Plasmids used to express NRD substrates....30
Figure 10: Target regions and primer sets used in RT-qPCR....35
Figure 11: Agarose gel of BY4741 transformants....44
Figure 12: Agarose gel of RNA isolated from NOY504 strain....46
Figure 13: Phenotypic analysis of NOY504::pSC1....50
Figure 14: Phenotypic analysis of NOY504::pWL160/155:pSC1....50
Figure 15: Microarray image generated with confocal microscopy....53

Figure 16: Raw and normalized 18S swapped microarray data.....55
Figure 17: Raw and normalized distribution of red and green intensities across all arrays.....55
Figure 18: Normalized 18S swapped microarray data.....56
Figure 19: Replicate plot of 18S swapped data….....58
Figure 20: MA plots of raw and normalized microarray data.....61
Figure 21: Distributions of red and green intensities during normalization in limma.....61
Figure 22: MA plot of microarray data following normalization in limma.....62
Figure 23: MA plot of microarray data following normalization in limma without background correction.....62
Figure 24: Replicate plots following normalization.....63
Figure 25: Cluster diagram of known genes in NRD.....63
Figure 26: Cluster diagram of previously identified genes.....65
Figure 27: Data normalization of microarray data in limma.....70
Figure 28: Replicate plots of microarray data following normalization.....70
Figure 29: Correlation matrix of first set of array replicates following normalization.....71
Figure 30: Correlation matrix of second set of array replicates following normalization.....71
Figure 31: Optimization of k-means clustering.....73
Figure 32: k-means cluster analysis of gene expression changes observed by microarray analysis.....74
Figure 33: GO term annotations of k-means clusters.....75
Figure 34: Analysis of known genes and previously identified genes.....76

**Abstract**

Nonfunctional ribosomal RNA decay (NRD) is a eukaryotic degradation pathway that targets and eliminates structurally intact but functionally defective ribosomal RNAs (rRNAs). Two separate NRD pathways for 18S and 25S rRNA have been identified. 18S NRD requires translation elongation and involves the termination factor-like proteins Hbs1p and Dom34p, and the mRNA decay factors Ski7p and Xrn1p. 25S NRD, however, is not dependent on translation elongation and requires the ubiquitin E3 ligase component Rtt101p and its associated protein Mms1p, as well as the ubiquitin-binding Cdc48 complex. Although identification of these factors has provided considerable insight into the degradation pathways, much remains to be uncovered. We have employed DNA microarrays to determine changes in gene expression that occur when defective rRNA substrates that activate NRD are present. These were analyzed with the goal of discovering additional factors involved in NRD. *Saccharomyces cerevisiae* cells were transformed with galactose-inducible plasmids containing NRD substrates. Activation of NRD was confirmed by RT-qPCR and phenotypic analysis. The mRNA population was then reverse transcribed to cDNA, labeled with fluorescent dyes, and hybridized to the microarray. Comparison of dye intensities allowed for determination of global gene expression changes induced by NRD. Initial data analysis revealed induction of ribosomal protein gene expression as well as rDNA silencing genes. Increased expression of ubiquitin was observed upon activation of 25S NRD, consistent with observations of ubiquitylated 25S NRD substrates. Repression of the deubiquitylation enzyme Otu1p and other RNA processing factors was also observed. Continued analysis of the microarray data and additional verification of potential genes of interest is an ongoing part of this investigation.

## Introduction and Background

Protein biogenesis involves the transcription of DNA to messenger RNA (mRNA) and the translation of mRNA into an amino acid sequence that ultimately becomes a protein. This process is known as the central dogma of molecular biology. Translation requires the ribosome, a large ribonucleoprotein complex that binds mRNA and incoming transfer RNAs (tRNAs) to synthesize a polypeptide. In a *Saccharomyces cerevisiae* cell, 80% of cellular RNA is ribosomal RNA (rRNA). A rapidly dividing yeast cell synthesizes ~1,000 ribosomes a minute and a fully mature cell contains approximately 200,000 ribosomes. In addition, rRNA transcription comprises 60% of total transcription and transcription of ribosomal proteins accounts for 50% of RNA Pol II activity. mRNAs encoding ribosomal proteins are also the substrate of 90% of mRNA splicing (Warner, 1999). Clearly, a large proportion of cellular resources are dedicated to ribosome synthesis and the importance of ribosomes in the cell demands accurate ribosome biogenesis and function.

The ribosome catalyzes mRNA decoding and polypeptide formation. The eukaryotic ribosome is composed of two subunits, the small (40S) subunit and the large (60S) subunit and contains 5,469 nucleotides of ribosomal RNA (rRNA) (Warner, 1999). In *Saccharomyces cerevisiae*, the small subunit is composed of the 18S rRNA and 33 proteins. The large subunit is composed of the 25S, 5S and 5.8S rRNAs and 46 proteins (Figure 1). The two subunits are connected by multiple intersubunit bridges formed by interactions between proteins and/or rRNA. At the subunit interface are three tRNA binding sites essential for translation: the A site, P site and E site (Ben-Shem et al., 2010).

The small subunit decoding center binds the mRNA and ensures recruitment of the appropriate tRNA. The mRNA coding region sequence contains instructions for protein synthesis

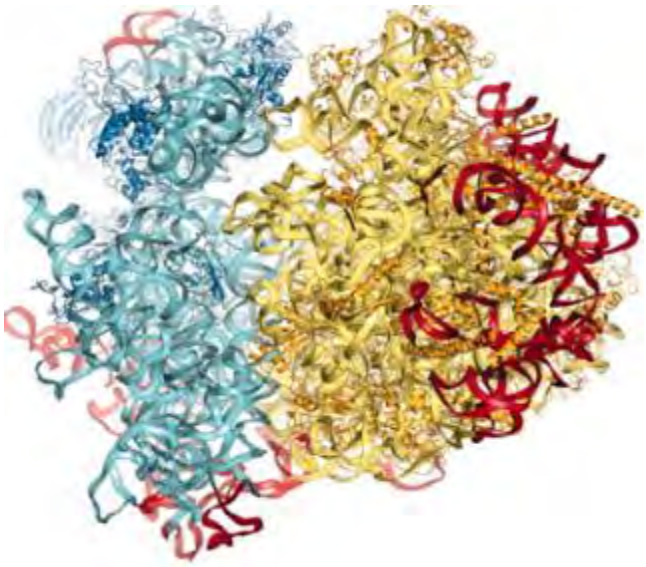

**Figure 1**: **Structure of the eukaryotic ribosome at 3.0 Å resolution.** Proteins and rRNA in the small subunit are shown in dark and light blue, respectively, and dark and pale yellow in the large subunit. Expansion segments consist of rRNA sequences inserted in the conserved rRNA core and are shown in red. These expansion elements are largely nonfunctional and account for the difference in length between eukaryotic and bacterial rRNAs (Ben-Shem et al., 2010).

and three base mRNA codons specify the next amino acid to be added to the polypeptide. The anticodon loops of incoming aminoacyl-tRNAs (aa-tRNAs) base pair to the mRNA codon and correct codon-anticodon interactions cause the addition of the next amino acid to the polypeptide. The large subunit active site catalyzes peptide bond formation by promoting nucleophilic attack of the incoming amino acid on the growing polypeptide chain. The ribosome is classified as a ribozyme since active sites of the ribosome are entirely composed of rRNA.

Ribosome Biogenesis

Ribosome biogenesis is a complicated process that requires the coordinated synthesis of rRNA and ribosomal proteins. Ribosomal RNA is transcribed inside the nucleolus and subjected to nuclear and cytoplasmic processing events. Biogenesis begins with transcription of a long precursor rRNA (35S pre-rRNA) that is subsequently processed into the mature 18S, 5.8S and 25S rRNAs (Figure 2). The 5S rRNA is transcribed separately and undergoes minimal processing prior to incorporation into in the large subunit. The 35S pre-rRNA contains the 5' external transcribed sequence (5'-ETS), 18S rRNA, internal transcribed spacer 1 (ITS1), 5.8S rRNA, ITS2, 28S rRNA and the 3'-ETS. During transcription, this transcript is rapidly cleaved in the 3'-ETS by endoribonuclease Rnt1p. Following transcription, the 35S pre-rRNA is subject to a host of modifications, such as pseudouridylation (conversion of uridine residues to pseudouridine) and 2'-O-ribose methylation. These modifications are mediated by various small nucleolar ribonucleoprotein particles (snoRNPs). Cleavages at sites $A_0$ and $A_1$ in the 5'-ETS yield the 33S and 32S pre-rRNA intermediates. Cleavage at site $A_2$ in ITS1 generates the 20S pre-rRNA and the $27SA_2$ pre-rRNA. The 20S pre-rRNA will eventually become the 18S rRNA and the $27SA_2$ pre-rRNA will become the 25S and 5.8S rRNAs. The 20S pre-rRNA is exported

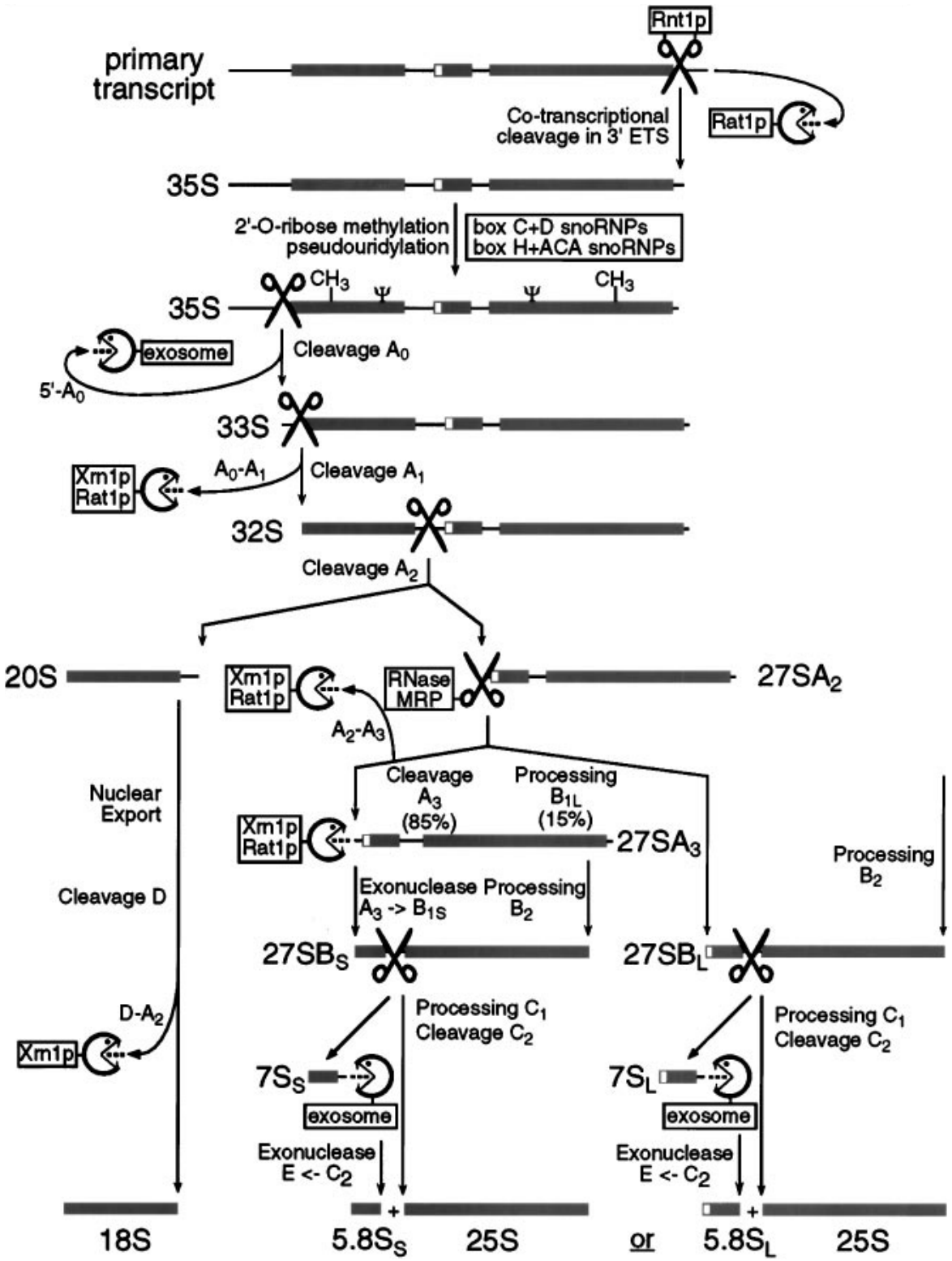


**Figure 2**: **Processing of pre-rRNA in *Saccharomyces cerevisiae*.** Ribosomal RNAs are transcribed as the long precursor 35S rRNA, which contains sequences that will become the mature 18S, 25S and 5.8S rRNAs. This transcript is subject to multiple cleavage and processing events. See text for details (Venema and Tollervey, 1999).

from the nucleus and subject to additional cleavage at site D at the 5' end of ITS1 to give the mature 18S rRNA (Venema and Tollervey, 1999). $27SA_2$ pre-rRNA processing can proceed by two alternative pathways. The major pathway involves cleavage at site $A_3$ in ITS1 by RNase MRP to the $27SA_3$ pre-rRNA. The $27SA_3$ pre-rRNA is then subject to exonucleolytic digestion to site $B_{1S}$ at the 5' end of mature 5.8S rRNA by Rat1p, yielding the $27SB_S$ precursor (Venema and Tollervey, 1999). The minor pathway involves processing at site $B_{IL}$ to produce the $27SB_L$ pre-rRNA. Precursors generated by both pathways are subject to additional processing at site $C_1$ and cleavage at site $C_2$ in ITS2 to give the 5.8S and 25S rRNAs (Venema and Tollervey, 1999).

These processing events occur in parallel with protein associations to form pre-ribosomal ribonucleoprotein (RNP) complexes (Figure 3). Simple association of rRNA with ribosomal proteins does not result in functional ribosomal subunits. Rather, the eukaryotic assembly pathway involves a large number of non-ribosomal proteins that are involved at different stages of ribosomal subunit maturation. Following transcription, the 35S transcript is quickly bound by at least four snoRNPs which catalyze early pre-rRNA cleavages, including U3 snoRNP. 90S pre-ribosome formation rapidly follows. The protein composition of this complex is very similar to the small subunit processome, an RNP complex required for 18S rRNA biogenesis. Essential proteins found in the 90S complex aid in $A_0$, $A_1$, and $A_2$ cleavages. These include Rrp5p, which is necessary for the $A_2$ cleavage. Although the 90S complex quickly splits into the pre-40S and pre-60S complexes following cleavages at $A_0$, $A_1$, and $A_2$, this complex contains proteins that are not found in its progeny. (Fromont-Racine et al., 2003).

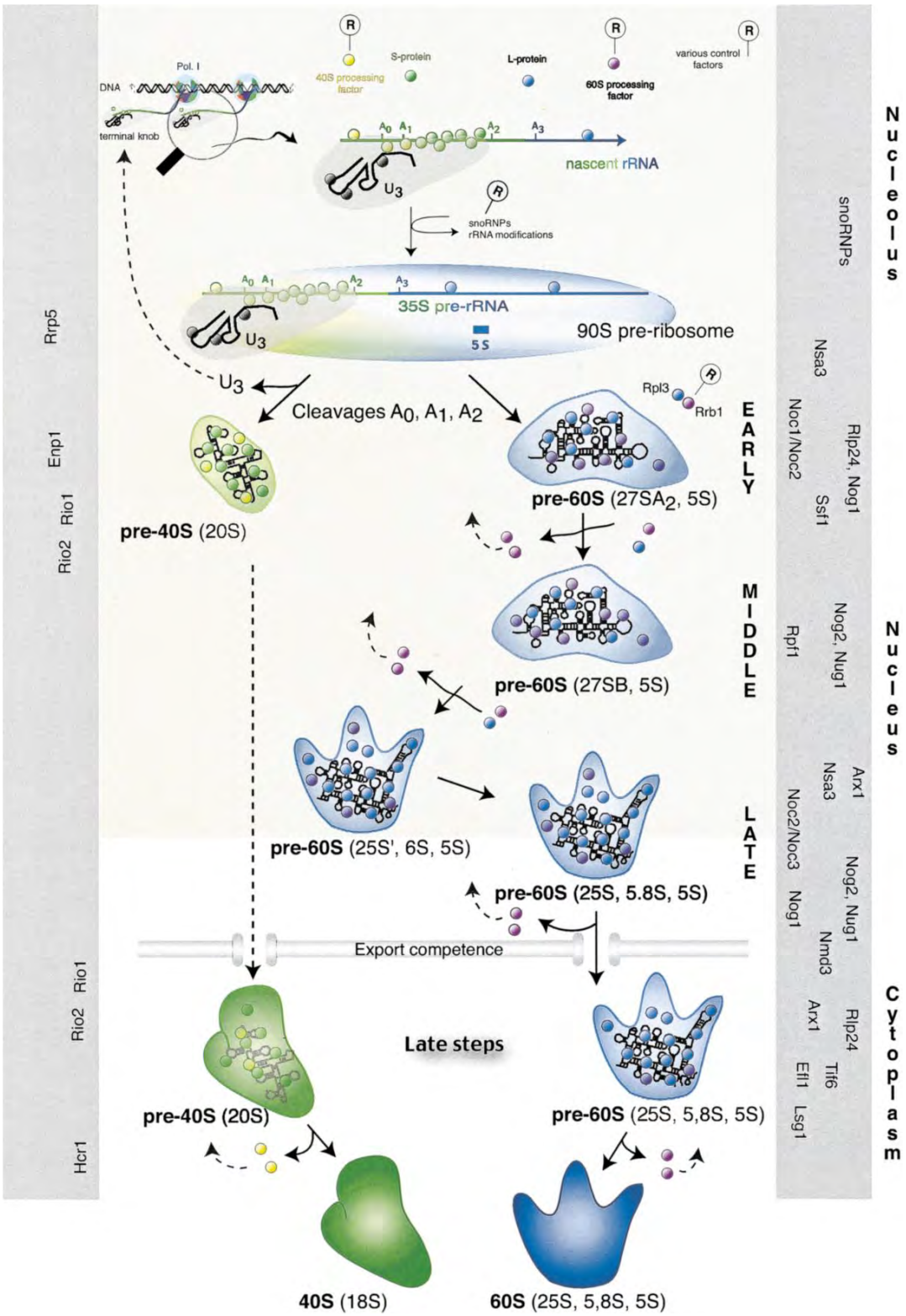


**Figure 3**: **Overview of the ribosome synthesis pathway.** Throughout processing, rRNA is bound by various proteins and other processing factors (i.e. snoRNPs) to form intermediate ribonucleoprotein complexes. These proteins can be catalytic or merely structural. See text for details (Fromont-Racine et al., 2003).

Although additional processing of the pre-60S subunit takes place in the nucleus, maturation of the pre-40S subunit takes place in the cytoplasm. Nob1p is associated with the pre-40S particle in the nucleus and accompanies the pre-ribosomal subunit during nuclear export. In the cytoplasm, Nob1p is responsible for cleavage at site D during 40S maturation (Fatica et al., 2003). The pre-40S complex is also known to contain essential kinases Rio1p and Rio2p. These two proteins associate with the pre-40S complex in the nucleus and accompany the complex into the cytoplasm. Although their phosphorylation targets are unknown, candidates include Rps31p and Rps6p, two 40S ribosomal proteins phosphorylated in yeast (Fromont-Racine et al., 2003). In the cytoplasm, Hcr1p, an eIF3-associated protein, is thought to influence the cleavage reaction at site D and also translation initiation (Fromont-Racine et al., 2003).

While some 40S processing factors are found in the 90S pre-ribosomal complex, 60S processing factors seem to associate after the 90S particle splits into the pre-40S and pre-60S complexes. One exception is Nsa3p, which is found in both 90S complexes and pre-60S complexes. Although many of the proteins found in pre-60S complexes have recently been discovered, it is unclear what their roles in processing may be. Structural similarities to ribosomal proteins found in mature ribosomal subunits suggest that some of these proteins may act as placeholders that bind rRNA at sites that will later be occupied. Upon export to the cytoplasm, additional processing is mediated by the GTPases Efl1p and Lsg1p. GTP hydrolysis by Efl1p helps release anti-associating factor Tif6p from the pre-60S complex. This allows for association with the small subunit. A similar role is proposed for Lsg1p, but the nucleolar factor it helps release is unknown. Nmd3p, a protein involved in export and quality control, is also thought to be important for large subunit recycling following translation (Fromont-Racine et al., 2003).

Translation

Translation is initiated when the small ribosomal subunit associates with mRNA in the cytosol and involves the interaction of numerous initiation factors (Figure 4). Initiation can begin once the ribosome is recycled from its previous round of translation (Figure 4, Step 1) and the eIF2 ternary complex is formed (Figure 4, Step 2). The eIF2 ternary complex consists of GTP-bound initiation factor eIF2 and the initiator tRNA Met-tRNA$^{Met}$. Met-tRNA$^{Met}$ initiates protein synthesis and places methionine as the first amino acid of the peptide. Prior to mRNA binding, the 40S subunit associates with the ternary complex eIF2·GTP·Met-tRNA$^{Met}$ and initiation factors eIF3, eIF1, eIF5 and eIF1A to form the 43S pre-initiation complex (Figure 4, Step 3). The mRNA is activated by associating with initiation factors eIF4F and eIF4B (Figure 4, Step 4).

RNA helicase activities of initiation factors eIF4F and eIF4B use ATP hydrolysis to unwind the secondary structures of the mRNA to aid in attachment. Small subunit attachment to the mRNA 5' cap is likely facilitated by interactions between eIF4G bound to the 5' end of the mRNA and eIF3 bound to the 43S complex (Figure 4, Step 5). The 43S pre-initiation complex now scans the mRNA until it reaches the start codon (Figure 4, Step 6). The AUG start codon is recognized by eIF1, which helps discriminate against incorrect start codons (Figure 4, Step 7). Upon recognition, the small subunit stalls and eIF5 binds to induce GTP hydrolysis and eIF2 dissociation. This leaves Met-tRNA$^{Met}$ bound to the P-site of the small subunit. eIF5, eIF3 and eIF1 also dissociate, allowing the 60S subunit to associate and form the complete 80S ribosomal complex (Figure 4, Step 8). The dissociation of these initiation factors and recruitment of the 60S subunit requires the GTPase eIF5B, which occupies the same site as eIF2. GTP hydrolysis

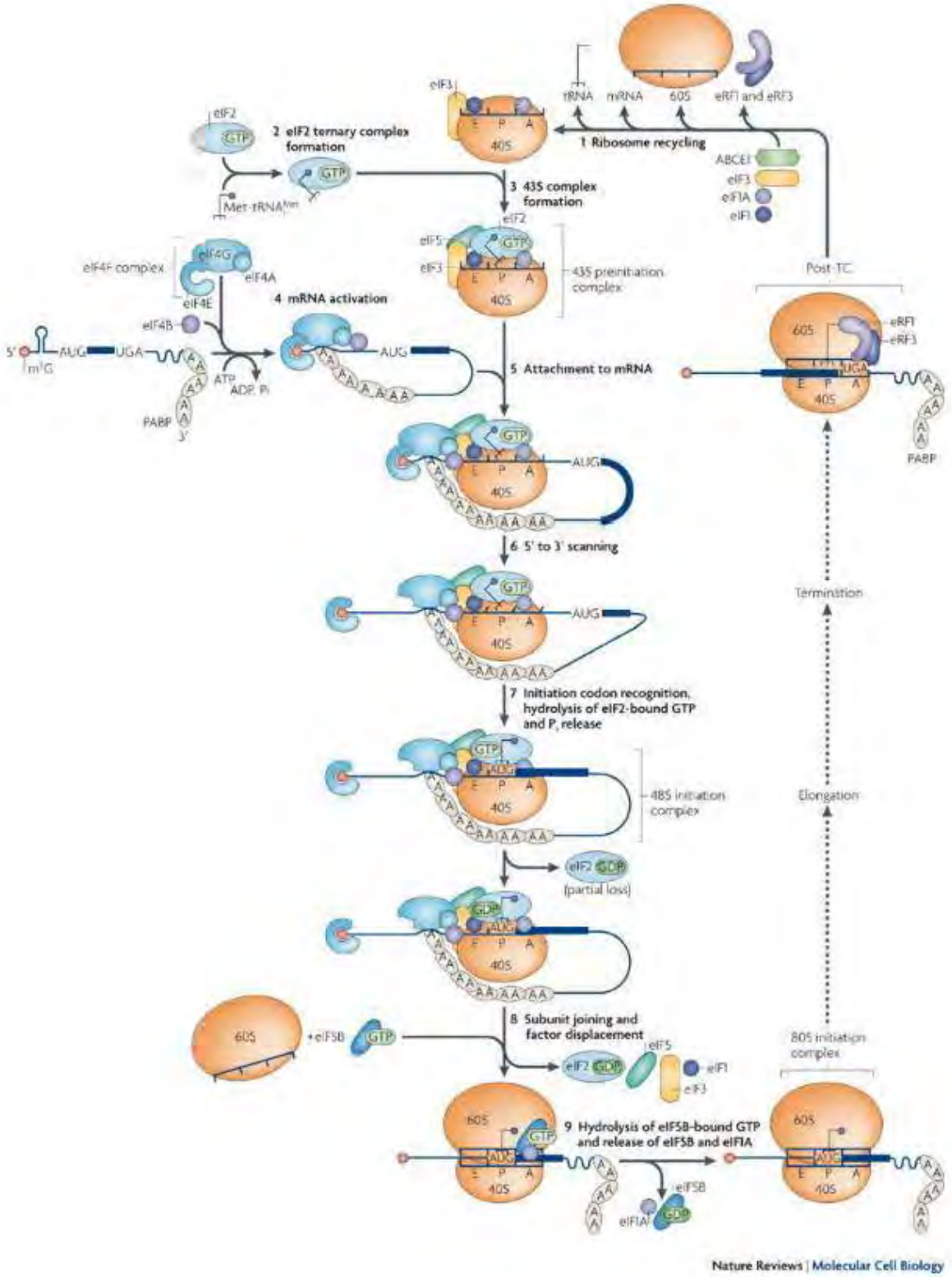


**Figure 4**: **Mechanism of translation initiation in eukaryotes.** Translation is initiated when the small subunit accompanied by initiation factors binds to an mRNA. This preinitiation complex scans the mRNA until it reaches the start codon, at which point the large subunit binds to form the functional 80S ribosomal complex. See text for details (Jackson et al., 2010).

by eIF5B catalyzes its release along with eIF1A release (Figure 4, Step 9). The 80S complex can now enter the elongation phase (Jackson et al., 2010).

Translation elongation constructs the polypeptide chain based on the instructions contained in the mRNA coding region. During elongation, tRNAs charged with amino acids are loaded into the A-site of the ribosome by the GTPase eEF1α (Figure 5). aa-tRNA delivery and codon recognition trigger GTP hydrolysis by eEF1α. The decoding site of the ribosomal small subunit ensures correct anticodon-codon interactions. Peptide bond formation is catalyzed by the peptidyl transferase center (PTC) of the large subunit and occurs by nucleophilic attack of the α-amino group of the A-site aa-tRNA on the peptidyl-tRNA in the P-site. Following peptide bond formation, ribosomal subunit ratcheting causes the tRNAs to shift into P/E and A/P hybrid states. In these hybrid states, the anticodon loops remain in the P and A site and the amino acid acceptor ends shift into the E and P sites. Translocation shifts the now uncharged tRNA into the E-site and the newly formed peptidyl-tRNA into the P-site. This step is catalyzed by the binding of the GTPase eEF2 in the A site. Rapid GTP hydrolysis unlocks the ribosome to allow mRNA and tRNA movement. Release of eEF2-GDP locks the subunits in place for the next round of elongation (Dever and Green, 2012).

When the ribosome reaches a stop codon, the release factor eRF1 binds to the A-site and recognizes the stop codon to catalyze the transfer of a water molecule to the end of the peptide chain (Figure 6). This releases the polypeptide from the ribosome and promotes ribosomal recycling. GTP hydrolysis by the release factor eRF3 accelerates peptide dissociation. Binding of ABCE1 is thought to promote ribosomal recycling following termination (Dever and Green, 2012).

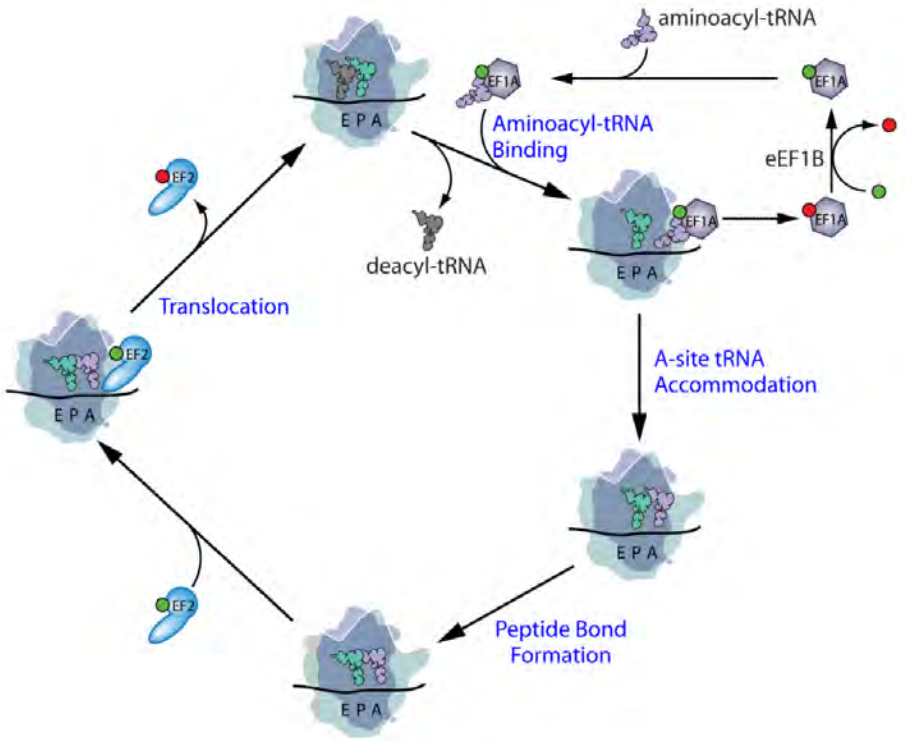


**Figure 5**: **Mechanism of translation elongation in eukaryotes.** Incoming aminoacyl-tRNAs are delivered to the ribosome by the GTPase eEF1α and bind to the A-site of the ribosome. The ribosome catalyzes peptide bond formation. Elongation factor eEF2 catalyzes translocation and release of the deacylated tRNA. See text for details (Dever and Green, 2012).

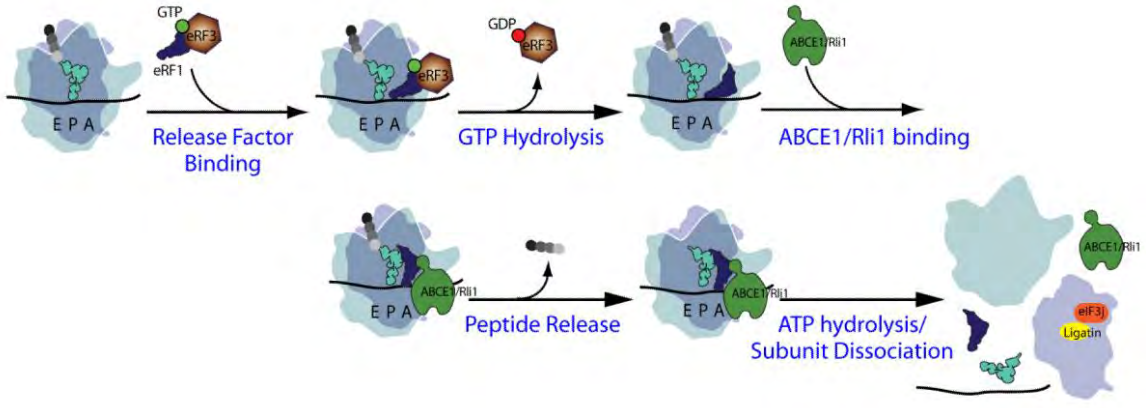


**Figure 6**: **Mechanism of translation termination in eukaryotes.** Upon stop codon recognition, eRF1 binds to the A site of the ribosome to catatalyze transfer of a water molecule to the end of the polypeptide. GTP hydrolysis by eRF3 accelerates peptide release and binding of ABCE1 promotes ribosome recycling (Dever and Green, 2012).

Ribosomal RNA Quality Control Mechanisms

Eukaryotic cells have developed RNA quality control mechanisms to enable accurate and energy efficient protein synthesis. Defective RNAs can be produced in a variety of ways including gene mutation, transcription errors, and RNA processing inaccuracies (Doma and Parker, 2007). Defective ribosomal RNA can cause the ribosome to stall during translation, preventing proper mRNA translation. In addition, defective RNAs may be implicated in disease pathology. For example, there is evidence of elevated levels of oxidized rRNA in patients with Alzheimer's disease (Ding et al., 2006). Therefore, degradation pathways to remove defective RNAs are essential to ensure normal cell function.

Prior to nuclear export, pre-rRNAs are subject to quality control mechanisms that target incorrectly processed pre-rRNAs. Inhibition of nuclear pre-rRNA processing factors should lead to an accumulation of pre-rRNAs, but this is not observed in all cases, indicating the existence of surveillance mechanisms (Lafontaine, 2010). One surveillance mechanism is mediated by the TRAMP-exosome pathway in which defective pre-rRNAs are polyadenylated by the poly(A) polymerase activity of the TRAMP complex. This complex is able to discriminate between defective and normal pre-rRNAs. Polyadenylated pre-rRNAs are subsequently degraded by the RNA exosome (Lafontaine, 2010). Additional RNase proteins can associate with this core complex to catalyze RNA degradation (Houseley et al., 2006).

Ribosomal RNA is covalently modified at specific bases by snoRNAs during nuclear processing. Many of these snoRNAs appear to be nonessential on their own and the subsequent modifications unnecessary for further processing. However, base dimethylation at the 3' end of 18S pre-rRNA by Dim1p is essential: knockdown of Dim1p prevents the modification and inhibits downstream pre-rRNA processing events (Lafontaine et al., 1998). This suggests the

existence of a quality control mechanism for 18S pre-rRNA that is inhibited by Dim1p. Moreover, Dim1p is recruited to 18S pre-rRNAs by Dim2p, a ribosomal RNA processing factor. Following Dim1p recruitment by Dim2p and base modification by Dim1p, the pre-40S subunit is marked for further pre-rRNA processing by downstream factors (Vanrobays et al., 2004).

Surveillance of ribosomal subunits also occurs during nuclear export, as is the case with a large subunit surveillance mechanism mediated by the nuclear export protein Nmd3p. Deletion of Nmd3p does not affect synthesis or processing of 25S rRNA, but mature 25S rRNA is rapidly degraded. These results implicate Nmd3p as an essential protein required for a late step of large subunit biogenesis (Ho and Johnson, 1999). Furthermore, Nmd3p binds mature 60S subunits and associates with an export receptor protein Crm1p to facilitate nuclear export. Deletion of the nuclear export signal sequence from Nmd3p resulted in an accumulation of 60S subunits inside the nucleus and inhibition of 60S subunit biogenesis (Ho et al., 2000).

Nonfunctional Ribosomal RNA Decay

While most surveillance mechanisms monitoring rRNA occur during processing and prior to nuclear export, nonfunctional rRNA decay (NRD) monitors mature rRNA (LaRiviere et al., 2006). Point mutations in the 18S rRNA decoding site and the 25S rRNA peptidyl transfer center can render the rRNA nonfunctional and these mutations are lethal in prokaryotes (Powers and Noller, 1990); (Thompson et al., 2001). However, in eukaryotes these defective rRNAs are degraded by NRD, rendering the mutations nonlethal. Typically, mature rRNAs are very stable with a half-life of several days (Lafontaine, 2010). Degradation by NRD results in significantly shorter rRNA half-lives for defective 18S rRNAs (~55 minutes) and defective 25S rRNAs (~75 minutes) (Cole et al., 2009). Polysome analysis shows defective 18S rRNA is found in mature

80S ribosomes, indicating that degradation occurs in the cytosol (LaRiviere et al., 2006). The long half-life of 25S rRNA determined by pulse-chase experiments exceeds the half-life of 25S rRNAs degraded during processing and degradation (such as Nmd3p dependent degradation), suggesting that 25S NRD occurs in the cytosol as well (LaRiviere et al., 2006).

While mutations in both 18S and 25S rRNA are degraded by NRD, the mechanisms behind this process for these two types of rRNA are very different (Figure 7). Fluorescent In Situ Hybridization (FISH) determined that nonfunctional 18S rRNAs are dispersed throughout the cytoplasm, while mutant 25S rRNAs are localized at distinct perinuclear foci (Cole et al., 2009). Furthermore, addition of translation inhibitor cycloheximide stabilizes 18S rRNA but not 25S rRNA. This indicates that degradation of 18S rRNA by NRD is translation dependent, consistent with the distribution observed by FISH (Cole et al., 2009).

18S NRD targets are also stabilized upon deletion of exonucleases Ski7p and Xrn1p, as well as mRNA decay proteins Hbs1p and Dom34p. A late-acting degradation pathway for mRNAs with stable secondary sequences that stall translation is No-Go Decay (NGD). This pathway also requires the same four protein factors (Doma and Parker, 2006). Dom34p and Hbs1p form a complex that is structurally similar to aa-tRNAs and is thought to bind the A-site of the ribosome to initiate degradation (Chen et al., 2010). Deletion of mRNA decay factors Dom34p and Hbs1p stabilize mutant 18S rRNA, but not 25S rRNA. This suggests that 18S NRD is mechanistically distinct from 25S NRD, but mechanistically similar to NGD. Further evidence for this relationship was suggested by localization of both 18S NRD and NGD substrates to P-bodies, cytosolic foci involved in mRNA turnover (Cole et al., 2009). However, certain mutations in Hbs1p disrupt interactions

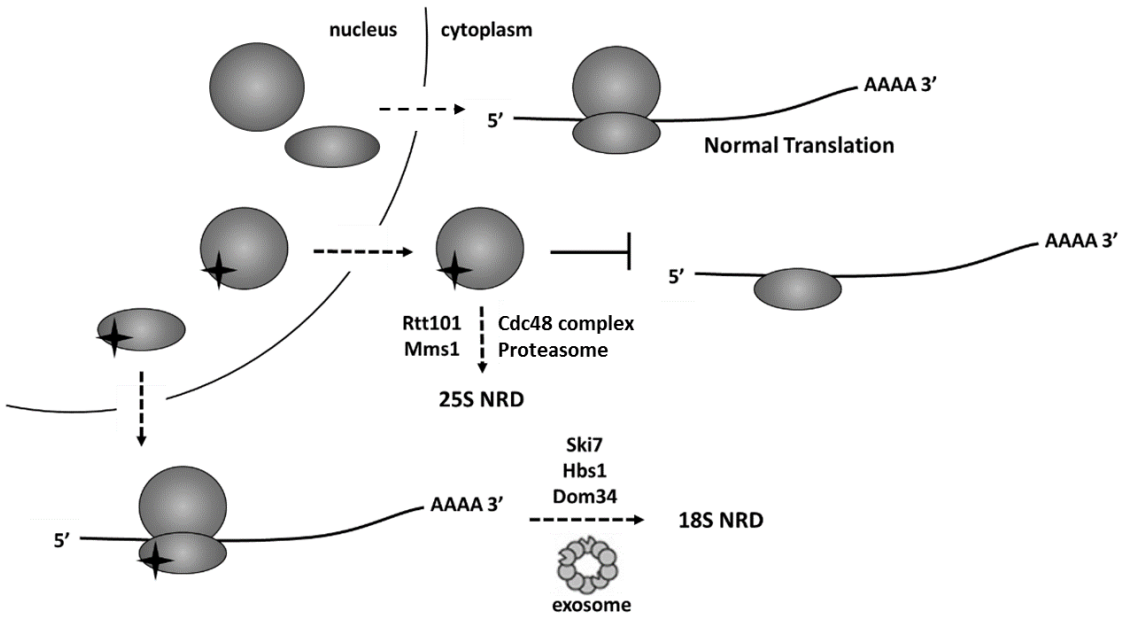


**Figure 7**: **Models for 18S NRD and 25S NRD.** Upon export from the nucleus, 18S NRD substrates are able to assemble into the small subunit. Defective 40S subunits associate with 60S subunits but the 80S complex stalls during mRNA translation. The stalled translation complexes are eliminated through the combined action of Dom34p, Hbs1p, Ski7p, Xrn1p, and the cytoplasmic exosome. Conversely, 25S NRD substrates accumulate around the nuclear envelope. They are eliminated after export to the cytoplasm by factors which include Rtt101p, Mms1p, the Cdc48 complex and the proteasome (modified from Cole et al., 2009).

between Dom34p and Hbs1p and strongly inhibit NGD, but have no effect on 18S NRD. This implies that the two pathways are distinct (Van Den Elzen et al., 2010).

Unlike 18S NRD, which shows mechanistic similarities to mRNA degradation pathways, 25S NRD is not affected by deletions of known exonucleases and other factors implicated in mRNA degradation. 25S NRD is also unaffected by deletion of exonuclease Rrp6, a component of the TRAMP-exosome pre-rRNA decay pathway. Protein factors involved in ubiquination by the GUARD complex, Rtt101 and Mms1, have been identified as essential for 25S NRD (Fujii et al., 2009). Furthermore, the ubiquitin-binding complex Cdc48-Npl4-Ufd1 (Cdc48 complex) and the proteasome are also involved in 25S NRD. The Cdc48 complex catalyzes dissociation of the 60S subunit from the 40S subunit prior to proteasome degradation. The proteasome is also essential for mutant 25S rRNA degradation (Fujii et al., 2012).

Identification of proteins such as Dom34p and Rtt101p allows insight into the individual mechanisms of RNA degradation pathways which require unique surveillance mechanisms. Further identification could offer insight into the fate of RNA targeted for degradation. For example, both mutant 18S rRNA and mutant mRNA are targeted for NRD and NGD and localize at P-bodies (Cole et al., 2009). However, the half-life of mutant 18S rRNA is approximately ten times longer than the half-life of mutant mRNA (Lafontaine, 2010). While this may be due to the relative complexity of rRNA, it may also be that 18S NRD is a two-step process. If this is the case, 18S NRD may involve different degradation factors than NGD which have yet to be identified (Cole et al., 2009). Identification of additional factors may be possible through the use of tools such as microarrays.

DNA Microarrays

DNA microarrays enable identification of gene expression changes caused by specific conditions or treatments. A microarray consists of rows of microscopic probes, each containing a small fragment of DNA coding for a specific gene. Microarrays enable observations of all transcribed mRNAs and comparison of wild-type to experimental condition cells. In our lab, the experimental condition is presence of NRD substrates that activate the degradation pathway. RNA isolated from both samples is reverse transcribed to cDNA, labeled using a fluorescent dye and hybridized to the microarray. Comparing the dye intensity between two samples reveals changes in gene expression which may allow for identification of genes involved in NRD. Due to dye bias based on different rates of degradation of the fluorescent dyes, a dye swap experiment is often performed where the same samples are labeled with the opposite dyes from the original experiment.

Preliminary NRD microarray data collection and analysis was previously performed (Lee, 2011). The microarray data from this experiment compares cells expressing plasmid-derived nonfunctional 18S rRNA to wild-type cells and nonfunctional 25S rRNA to wild-type cells. A dye swap experiment was also performed to take into account any difference in dye intensity. This data was imaged by the Genome Consortium for Active Teaching (GCAT) at Davidson College and analyzed using GCAT's MAGIC Tool (Heyer et al., 2005). Preliminary analysis ranked expression ratios based on relative dye intensities (Figure 8). Of the top five induced and repressed genes examined, none of the top five induced genes for 18S NRD are known to be involved in processes that may relate to rRNA degradation. However, since genes can perform various functions within the cell, future studies may demonstrate involvement in NRD.

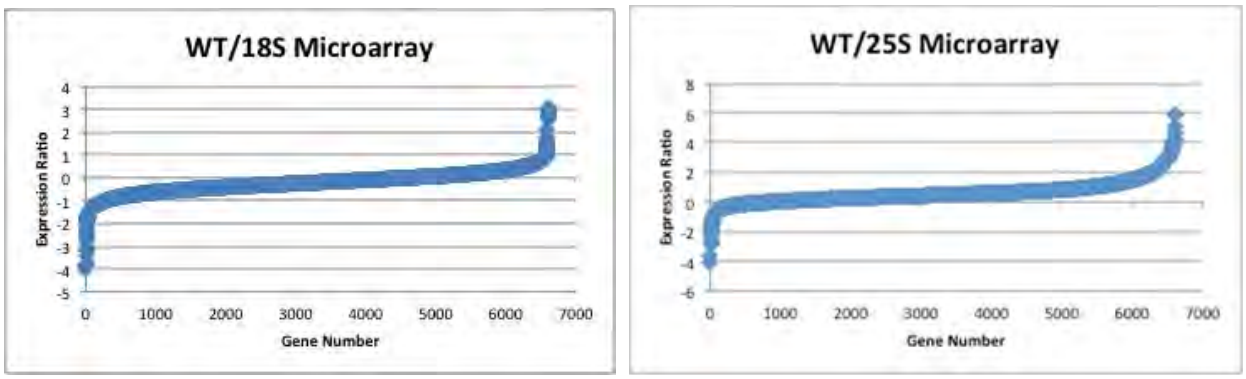


**Figure 8**: **Expression ratios for normal WT/18S microarray and WT/25S microarray.** Each gene is assigned an arbitrary number and ranked in order to expression ratio. Genes with the most positive expression ratios are induced and genes with the most negative expression ratios are repressed (Lee, 2011).

For 18S NRD and 25S NRD, genes involved in nucleotide de novo biosynthesis were repressed (Lee, 2011). Repression of these genes could indicate that NRD produces an excess of nucleotides within the cell, eliminating the need for de novo biosynthesis.

Additionally, a gene involved in formation of the ribosomal stalk is repressed during 18S NRD (Lee, 2011). The ribosomal stalk is involved in ribosome binding to translation elongation factors. Repression of this gene during 18S NRD may indicate that the ribosome does not have contact with translation elongation factors when it becomes stalled on the mRNA strand. Several genes encoding ribosomal proteins were also found to be induced in 25S NRD (Lee, 2011). This may indicate that rRNA degradation by NRD causes increased expression of ribosomal proteins, which may also be degraded by NRD.

Preliminary analysis also identified YLR243W. This is a gene of unknown function whose expression is repressed in both 18S NRD and 25S NRD (Lee, 2011). However, because this gene is essential to cell survival, it would be difficult to test in a knock-out strain. Involvement of YLR243W in NRD could suggest a link between 18S and 25S NRD, where previously no link had been identified. Identification of the function of YLR243W may aid in establishing this hypothesis.

Project Purpose

The goals of this current project were twofold: (1) to further analyze the existing microarray data using more sophisticated normalization and statistical analyses and (2) to conduct another microarray experiment. The initial microarray data had low signal intensity. This was presumably caused by a number of factors including microarray processing and dye labeling techniques. The initial microarray experiment was shipped to Davidson College for

scanning, during which time the photosensitive Cy3 and Cy5 dyes may degrade. This is especially a concern for the Cy5 dye, which is unstable and reacts rapidly with ozone present in the air (Fare et al., 2003). To resolve this, further microarray experiments were scanned on-site using an Olympus IX51 inverted laser scanning confocal microscope. Additionally, the original cDNA labeling protocol involved end-labeling the cDNA oligos with a fluorescently labeled dendrimer nanomolecule (Genisphere). For future microarray studies, we adopted the traditional method of incorporating aminoallyl-dUTP (aa-dUTP) into the cDNA synthesis reaction (Inada and Pleiss, 2010). The aa-dUTP can then be coupled to the Cy dyes to incorporate multiple dye molecules per oligo. These alternative methods were put in place to increase the signal-to-noise ratio, allowing for more robust data collection. We also investigated the NOY504 strain for use in microarray analysis, which allows for increased relative expression of NRD substrates. In typical yeast strains, the ratio of plasmid-derived rRNA to chromosomally-derived rRNA is as low as 1:100 (LaRiviere et al., 2006). The NOY504 contains a temperature sensitive mutation which allows for shut-off of chromosomally-derived rRNA, allowing us to achieve a ratio of defective rRNA to functional rRNA closer to 50:50. With these new techniques and modifications, we sought to accurately determine differentially expressed genes during activation of NRD which may be involved in the degradation pathway. Identification of additional factors involved in NRD will ultimately contribute to a more complete understanding of this quality control mechanism and its biological implications.

## Materials and Methods

Yeast Culturing

All yeast strains (Table 1), unless otherwise noted, were struck out from frozen glycerol stocks onto solid YPD agar plates (1% yeast extract, 2% glucose, 2% peptone, 2% agar in $dH_2O$, autoclaved). Plates were then incubated at 30°C for two to three days until single colonies appeared. These single colonies were used to inoculate liquid YPD cultures (1% yeast extract, 2% glucose, 2% peptone in $dH_2O$, autoclaved). Liquid cultures were incubated at 30°C in a shaking incubator at 275 rpm until the cultures reached saturated cell densities. The NOY504 strain was incubated at 25°C until immediately prior to RNA isolation or phenotypic analysis. At this time, the cultures were grown at 37°C to shut off endogenous rRNA expression (see section below). Cell density was monitored by measuring the absorbance at 600 nm ($A_{600}$). Saturation corresponds to an $A_{600}$ reading of between 6-10 $A_{600}$ for untransformed yeast strains and an optical density reading of between 4-6 $A_{600}$ for transformed yeast strains.

**Table 1: Yeast strains used in this study.**

| Yeast Strain | Genotype | Source |
|---|---|---|
| BY4741 | MAT a his3Δ1 leu2Δ0 met15Δ0 ura3Δ0 | Open Biosystems |
| NOY504 | MAT α ade2-101 ura3-1 trp1-1 leu2-3,112 can1-100 rrn4::LEU2 | (Nogi et al., 1993) |

Other media used in this study include:

$Ura^-$ Glucose (1X yeast nitrogen base (YNB) (6.7 g/L), 1X Ura dropout supplement (1.92 g/L), 2% glucose in $dH_2O$, autoclaved)

$Ura^-$ Glucose plates (1X yeast nitrogen base (YNB) (6.7 g/L), 1X Ura dropout supplement (1.92 g/L), 2% glucose, 2% agar in $dH_2O$, autoclaved)

$Ura^-$ Raffinose (1X yeast nitrogen base (YNB) (6.7 g/L), 1X Ura dropout supplement (1.92 g/L), 2% raffinose in $dH_2O$, autoclaved)

$Ura^-$ Galactose (1X yeast nitrogen base (YNB) (6.7 g/L), 1X Ura dropout supplement (1.92 g/L), 2% galactose in $dH_2O$, autoclaved)

Ura$^-$ Trp$^-$ Glucose (1X yeast nitrogen base (YNB) (6.7 g/L), 1X Ura, Trp dropout supplement (0.72 g/L), 2% glucose in $dH_2O$, autoclaved)
Ura$^-$ Trp$^-$ Glucose plates (1X yeast nitrogen base (YNB) (6.7 g/L), 1X Ura, Trp dropout supplement (0.72 g/L), 2% glucose, 2% agar in $dH_2O$, autoclaved)
Ura$^-$ Trp$^-$ Raffinose (1X yeast nitrogen base (YNB) (6.7 g/L), 1X Ura, Trp dropout supplement (0.72 g/L), 2% raffinose in $dH_2O$, autoclaved)
Ura$^-$ Trp$^-$ Galactose (1X yeast nitrogen base (YNB) (6.7 g/L), 1X Ura, Trp dropout supplement (0.72 g/L), 2% galactose in $dH_2O$, autoclaved)

Phenotypic growth analysis was also performed for the NOY504 strain. Ura$^-$ and Ura$^-$ Trp$^-$ raffinose cultures of the NOY504 transformants were grown to an $OD_{600}$ reading of 1.0. A dilution series of five 5-fold dilutions was plated in 5 µL aliquots on Ura$^-$ and Ura$^-$ Trp$^-$ plates. Six experimental plates were incubated at various temperatures: Ura$^-$ and Ura$^-$ Trp$^-$ glucose at 25°C, 30°C, and 37°C, Ura$^-$ and Ura$^-$ Trp$^-$ galactose at 25°C, 30°C, and 37°C.

NOY504 Strain

Interest in the NOY504 strain of yeast was motivated by the low signal strength of previous microarray experiments, which is thought to be caused by the excess of endogenous rRNA in relation to plasmid-derived rRNA. The NOY504 strain allows for expression of endogenous rRNA to be shut off. This amplifies the effect of NRD on gene expression since a larger proportion of the rRNA population are substrates for NRD. NOY504 is a temperature sensitive strain; at 25ºC endogenous DNA is expressed, but at 37ºC all rRNA in the cell is plasmid-derived. Before use in microarray experiments, plasmid expression in this strain was examined through RT-qPCR and phenotypic analysis.

NRD Substrate Expression Plasmids

To induce NRD in cells, our lab employs galactose inducible plasmids to drive the expression of defective 18S and 25S rRNA (Table 2). The pSC1 plasmids (Figure 9A) also contain a gene that codes for the production of uracil, which allows transformed cells to grow on plates lacking uracil. The plasmids also contain a unique sequence tag which allows for discrimination between plasmid-derived and chromosomally-derived rRNA during RT-qPCR analysis. A sequence tag is a short nucleotide sequence that is incorporated into the rRNA transcript and corresponds to primers used during RT-qPCR. The pSC1-WT plasmid is used as a control in analysis and contains genes that code for functioning 25S and 18S rRNAs (Figure 9A). The pSC1-18S and pSC1-25S plasmids contain point mutations in the 18S rRNA decoding site and the 25S rRNA peptidyl transfer center that induce 18S and 25S NRD (Figure 9B,C). The pSC1-DM plasmid includes both of these point mutations to induce both NRD pathways (Figure 9D).

**Table 2: Plasmids used in this study.**

| Plasmid | Description | Source |
|---|---|---|
| pSC1-WT | URA3, 2μ, GAL7-rDNA | (Cole et al., 2009) |
| pSC1-18S | URA3, 2μ, GAL7-rDNA 18S:A1492C | (Cole et al., 2009) |
| pSC1-25S | URA3, 2μ, GAL7-rDNA 25S:U2585A | (Cole et al., 2009) |
| pSC1-DM | URA3, 2μ, GAL7-rDNA 18S:A1492C 25S:U2585A | LaRiviere, unpublished |
| pWL160 | TRP1, 2u, GAL7-rDNA | (Liang et al., 1997) |
| pWL155 | TRP1, 2u, GAL7-rDNA | (Liang et al., 1997) |

Our experiments with NOY504 necessitated the use of two additional plasmids that contain a gene encoding for tryptophan instead of for uracil (Figure 9E,F). This allowed for transformation of the NOY504 strain with two plasmids: one encoding wild-type rRNA so that the strain could grow at 37°C without the need for endogenous rDNA expression and one encoding mutant rRNA to activate NRD. This way, the percentage of transcribed mutant rRNA

in the cell should be closer to 50% rather than 1%, as in typical yeast strains. The pWL160 plasmid encodes for functioning 18S and 25S rRNAs with identical sequence tags to the pSC1 plasmids (Figure 9E). The pWL155 plasmid also encodes for functioning rRNAs, but with different sequence tags that do not show up in RT-qPCR (Figure 9F).

Yeast Transformation

In order to observe NRD, plasmids were transformed that express mutant 18S and 25S rRNAs. Cells were struck out on solid YPD plates from -80°C stocks, and single colonies were used to inoculate liquid 5 mL YPD cultures which were incubated in a rotary shaker at 275 rpm and 30°C. These cultures were grown to an $OD_{600}$ reading of 5.0 and were used to inoculate a 25 mL YPD culture. This YPD culture was incubated in the shaker for at least two doubling times (~1.5 hours) until it reached on $OD_{600}$ of 0.5-1.0. This culture was transferred to a 50 mL conical tube and centrifuged at 3000 rpm for five minutes to pellet cells. The supernatant was removed and the pellet was washed in 25 mL of 10mM sterile Tris-HCl (pH 7.5). The resulting pellet was resuspended in 12.5 mL sterile LiT (10mM Tris-HCl (pH 7.5), 100mM LiOAc, filter sterilized with a .20 μm filter) and 125 μL sterile 1M dithiothreitol (DTT). The cells were then incubated at room temperature for 40 minutes with gentle shaking. While cells were incubating, the polyethylene glycol (PEG) solution and transformation tubes were prepared. The PEG solution was prepared by combing 2 g PEG 3500 and 2 mL sterile LiT in a 10 mL conical, which was secured onto a vortex with tape to dissolve the PEG. The solution was filter sterilized using a .45 μm filter prior to use. Each transformation tube contained 50 μL sterile LiT, 5 μL SS carrier DNA, and 1 μg plasmid DNA. A control transformation tube without plasmid DNA was also included. After the 40 minute incubation, the cells were spun down by centrifuging at 3500 rpm

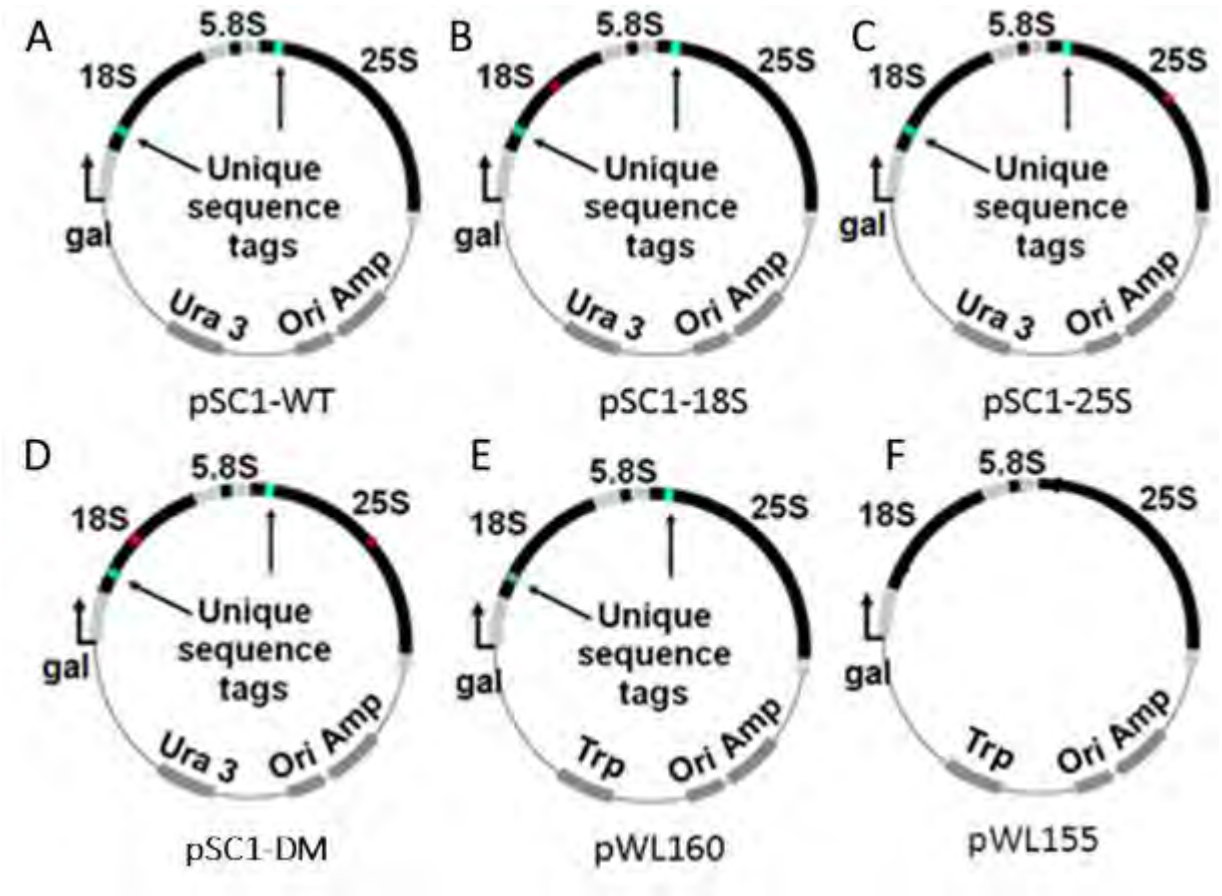


**Figure 9: Plasmids used to express NRD substrates.** Blue indicates unique sequence tags used for RT-qPCR analysis and red indicates point mutations used to induce NRD. Bent arrow indicates transcription start site. Ori indicates origin of plasmid replication and Amp indicates gene responsible for ampicillin resistance during bacterial plasmid production. Ura and Trp indicate additional genes responsible for uracil and tryptophan production. A-D) pSC1 plasmids E) pWL160 plasmid F) pWL155 plasmid.

for 5 minutes. The supernatant was discarded and the cells resuspended in 0.75 mL sterile LiT and 7.5 μL sterile 1M DTT. One hundred microliters of competent cells were added to each transformation tube and the tubes were incubated at room temperature for 10 minutes. Following this incubation, 300 μL of PEG solution was added to each tube, and the tubes were then incubated at room temperature for 10 minutes. After ten minutes at room temperature, 50 μL DMSO was added to each transformation tube. The transformation tubes were then incubated at 42°C for 15 minutes. Following this incubation, the cells were spun at 6000 rpm for 30 seconds. The supernatant was then removed and the cells resuspended in 1 mL YPD media. The tubes were incubated at 30°C for one hour, followed by centrifugation at 6000 rpm for one minute. The supernatant was removed and the cells resuspended in 500 μL of YPD media. One hundred microliters of this reaction was plated on dropout glucose plates, which were incubated at 30°C for two to four days. The resulting colonies were used to inoculate five mL cultures of dropout raffinose medium. The glucose cultures were used to inoculate dropout galactose cultures to induce plasmid expression. RNA was isolated from these galactose cultures. For NOY504 cultures, all incubation temperatures were kept at 25°C until transfer to galactose media, when cultures were incubated at 37°C.

RNA Isolation

To observe rRNA levels for verification of NRD activation and to isolate the mRNA population for microarray analysis, RNA must be isolated from the cells. The 5 mL galactose cultures of tranformants were transferred to 15 mL conical tubes, centrifuged for five minutes at 3500 rpm, and the supernatant discarded. The pellets were resuspended in 500 μL of AE buffer (50mM NaOAc, 10mM EDTA, pH 5.5) and transferred to 1.5 mL microcentrifuge tubes. The

tubes were centrifuged for five minutes at 3500 rpm and the supernatant removed. The pellets were resuspended in 450 μL of AE Buffer. Fifty microliters of 10% sodium dodecyl sulfate (SDS) was added and tubes vortexed for 10 seconds. In the hood, 500 μL of phenol (pH 4.2) was added and tubes vortexed for 10 seconds, twice. The tubes were incubated at 65°C for five minutes, vortexed for 5 seconds every 30 seconds. The tubes were cooled to room temperature by briefly placing in liquid nitrogen and then centrifuged for five minutes at 13,000 rpm. The aqueous phase (~500 μL) was transferred to a fresh 1.5 mL microcentrifuge tube. Five hundred microliters of phenol/chloroform/isoamyl alcohol (pH 4.2) was added to new tubes and vortexed for 10 seconds, twice. The tubes were centrifuged for five minutes at 13,000 rpm and the aqueous phase (~450 μL) transferred to a fresh 1.5 mL microcentrifuge tube. If solution wasn't clear, the phenol/chloroform/isoamyl alcohol addition was repeated. Five hundred microliters of chloroform was added, and mixture vortexed for 10 seconds, twice. The tubes were centrifuged for five minutes at 13,000 rpm and the aqueous phase (~400 μL) transferred to a fresh 1.5 mL microcentrifuge tube. 5 PRIME phase-lock gel tubes were used as an alternative for this portion of the RNA isolation protocol. For the phase-lock protocol, two additions of phenol/chloroform/isoamyl alcohol (pH 4.2) were made instead of the initial phenol addition followed by addition of phenol/chloroform/isoamyl alcohol. The phenol/chloroform/isoamyl alcohol was added and incubated at 65°C for five minutes as before. Following the incubation the mixture was transferred to the phase-lock tube and the protocol was followed as stated previously, except that the organic phase remained in the phase-lock tube after each step. The phase-lock tubes were used according to the manufacturer's protocol (5 PRIME). Forty microliters of 3M NaOAc (pH 5.2) was added to each tube and mixture vortexed. One milliliter of 100% ethanol was added to each tube and mixture vortexed well. Tubes were placed at -80°C

for one hour, then spun at 13,000 rpm for five minutes, and supernatant removed. The pellet was washed with 500 μL 70% ethanol, spun at 13,000 rpm for 15 minutes, and supernatant removed. The pellets were then dried in the speedvac and resuspended in 25 μL of sterile water. The RNA concentrations were determined using a Nanodrop spectrophotometer.

Agarose Gel Electrophoresis

Agarose gel electrophoresis was used to determine the integrity of the RNA isolated from the transformants. Five micrograms of RNA from each sample was run on the agarose gel. The total volume was brought up to 10 μL with 0.5X TBE (40mM Tris-HCl, pH 8.3, 45 mM boric acid, 1 mM EDTA), and 2 μL of loading dye was added to each sample. The gel was poured using 80 mL of 1% agarose and 0.5X TBE, microwaved to dissolve agarose. The gel was run at 100 Volts for ~1 hour. The gel was stained in an ethidium bromide solution for five minutes, then destained in water and imaged using a gel documentation system.

RT-qPCR

After confirming that the 18S and 25S rRNA remained intact in our samples, cDNA was synthesized from the RNA. This cDNA is used in the RT-qPCR reaction, since the enzyme responsible for signal amplification, Taq polymerase, acts on DNA substrates. First the RNA was DNase treated to remove any remaining DNA. Based on the RNA concentrations determined using the nanodrop, aliquots were used corresponding to 5 μg of RNA sample. The DNase reaction consisted of 5 μg of RNA, 1 μL 10X DNase buffer, 4 μL RQ1 DNase (1U/μL) and sterile water, for a total reaction volume of 10 μL. This reaction was allowed to incubate at 37°C for 30 minutes. One microliter of stop buffer (20 mM ethylene glycol tetraacetic acid,

EGTA) was added to each sample and the DNase was inactivated by incubating at 65°C for 10 minutes.

The DNase-treated RNA was then annealed to primers by adding DNase-treated RNA to the RNA/Primer Mix and heating at 60°C for five minutes. RNA/Primer Mix consisted of 1.25 μL $dN_9$ (4g/L), 5.5 μL DNase-treated RNA and 3.25 μL sterile water. The reaction was allowed to cool slowly on the benchtop for 15-30 minutes. The cDNA synthesis reaction was initiated by adding 10 μL enzyme/dNTP mix and allowed to proceed in 42°C water bath overnight. The enzyme/dNTP mix consisted of 4 μL RT buffer (5X First Strand buffer), 2 μL DTT (100 mM), 1 μL dNTPs (10 mM each), 0.5 μL RT (Clontech SMART MMLV RT, 200 U/μL), and 2.5 μL sterile water.

The RT-qPCR reaction allows us to determine relative quantities of plasmid-derived rRNA based on the amplification of the cDNA sample by Taq polymerase using plasmid-specific primers (Figure 10). The RT-qPCR reaction was carried out in a 96-well plate using a BioRad thermocycler. Each well contained a 20 μL reaction, made up of 5 μL of diluted cDNA, 5 μL of primer mix (4X, 1 μM), and 10 μL of BioRad iQ SYBR Green Supermix. The cDNA was diluted to a concentration of 2 ng/μL in Tris-HCl (pH 8.5) to get 10 ng of cDNA per reaction. The primer mix contains forward and reverse primers at a concentration of 1 μM each for a final concentration of 250 nM each (Table 3).

Once the wells were filled, the plate was centrifuged using a swing bucket rotor at 2500xg. Quantification the RT-qPCR results was performed using previously determined standard curves to quantify the starting concentration of template. This value is divided by the concentration of uracil template and normalized to wild-type values to obtain a relative fold difference.

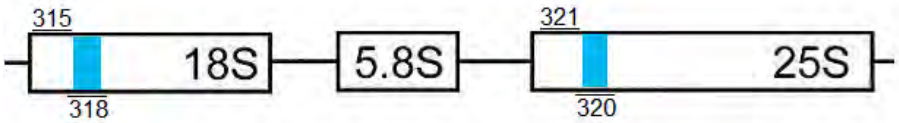


| Target Regions | Primer Sets |
|---|---|
| Tagged 18S rRNA | 315/318 |
| Tagged 25S rRNA | 321/320 |
| URA gene | 325/326 |

**Figure 10: Target regions and primer sets used in RT-qPCR.** 35S pre-rRNA shown at top of figure, containing 18S, 5.8S and 25S rRNA sequences. Blue regions indicate sequence tags. Target regions corresponds to RT-qPCR primers indicated by numbers above and below 35S pre-rRNA (Lee, 2011).

**Table 3: Primer sets used for RT-qPCR analysis.**

| Primer Set | Oligonucleotide sequences |
|---|---|
| 18S: 315/318 | 5'TCTGGTTGATCCTGCCAGTAGTCAT/<br>5'AAAGCGAGGATCCAGGCTTTGGTCG |
| 25S: 321/320 | 5'GGTACTGAAGCTCTCGAGTGTACCT/<br>5'TACCACCCACTTAGAGCTGCATTCC |
| URA: 325/326 | 5'GTTTAGATGACAAGGGAGACGCATT/<br>5'CTCTACCTTAGCATCCCTTCCCTTT |

cDNA Synthesis for aa-dUTP Labeled Microarray Analysis

The RNA used in the cDNA synthesis for microarray analysis was not DNase treated. Five micrograms of RNA was annealed to primers by adding to RNA/Primer Mix and heating at 70°C for five minutes. RNA/Primer mix consisted of 6.5 µL $dN_9$ (4g/L), 50 µg RNA and sterile water for a total reaction volume of 50 µL. The reaction was allowed to cool slowly on the benchtop for five minutes. The cDNA synthesis reaction was initiated by adding 50 µL enzyme/dNTP mix and allowed to proceed in 42°C water bath for 2-4 hours (reaction 90% complete after 2 hours). Enzyme/dNTP mix consisted of 20 µL RT Buffer (5X First Strand buffer), 10 µL DTT (100 mM), 5 µL dNTPs + aminoallyl-dUTP (10mM dATP, dCTP, dGTP; 6mM dTTP; 4mM aa-dUTP), 2.5 µL RT (Clontech SMART MMLV RT, 200 U/µL), and 12.5 µL sterile water. The reactions were stopped by adding 50 µL hydrolysis buffer (0.3M NaOH, 0.03 M EDTA) to each reaction. The reactions were incubated at 65°C for ten minutes.

cDNA samples for microarray analysis were purified using a Zymo DNA cleanup kit 25-Clean-and-Concentrate. Two volumes of DNA binding buffer was added to each sample and the sample was loaded on to a Zymo column and spun in a microcentrifuge for one minute at 13,000 rpm. The flowthrough was discarded and 200 µL wash buffer was added and the sample spun again. The column was then moved to a fresh microcentrifuge tube and 40 µL water added to the column. The column was allowed to sit at room temperature for one minute and then spun again. The eluent was dried in a speedvac and stored in the freezer.

Dye-Coupling and Array Hybridization for aa-dUTP Labeled Microarray Analysis

Prior to hybridization, arrays were hydrated to allow for even hybridization and blocked to prevent nonspecific hybridization. For array hydration, a large shallow Tupperware container

was filled with a 1 cm deep slurry of saturated NaCl (35g/100mL). The saturated NaCl in a sealed container creates a relative humidity of 75% to hydrate the spots. Arrays were placed in a plastic slide box and set in Tupperware container so that it floated on top of the slurry. The container was sealed and slides left to hydrate for 24 to 72 hours. Slides were then blocked using succinic anhydride, which reacts with the exposed poly-L-lysine coating on the array to prevent nonspecific binding of labeled cDNA. For the blocking reaction, 70 mL of 1-methyl-2-pyrrolidinone was measured into a clean, dry beaker. Then 1.15 g of succinic anhydride was dissolved, immediately followed by the addition of 3.1 mL of 1M sodium borate (pH 8.0). The buffered blocking solution was quickly poured into a clean, dry hybridization chamber. Arrays were placed in the chamber and vigorously shaken for 30 seconds. The chamber was then moved to a rotator and shaken for 15 minutes. Slides were transferred to a plastic slide box and washed thoroughly with Milli-Q water three to four times with vigorous shaking. Following this wash, slides were transferred to a dish containing 95% ethanol, plunged several times, and dried by centrifugation for three minutes at 500 rpm.

cDNA pellets post-cleanup were resuspended in 5 μL 0.1 M sodium bicarbonate (pH 9.0). After this point, all future preparation was done in the dark. Dye aliquots were prepared by resuspending one dye pack in 46 μL DMSO. Five microliters of dye were used to label cDNAs. Cy3 dye was used to label sample containing wild-type plasmid, and Cy5 dye was used to label sample containing mutant plasmid. This was reversed in the dye swap arrays. Samples were incubated at 60°C for one hour. Samples were then cleaned up using procedure described above. The two samples were combined before drying down in speedvac. The sample was then resuspended in 39 μL dd$H_2O$ and heated at 90°C for 5 minutes. To the resuspended sample, 0.5 μL 1M Hepes (pH 7.0), 3.5 μL 20X SSC, 1 μL 10 mg/mL poly(A) and 0.5 μL of 10% SDS were

added. The sample was placed on slide and coverslip applied. Ten microliters of 3X SSC was placed on slide label. The slide was then placed in hybridization chamber at 37°C for 24 hours.

The slide was removed from hybridization chamber and submerged in Wash I (340 mL water, 10 mL 20X SSC, 1 mL 10% SDS) to gently remove coverslip. The slide was then incubated in Wash I with vigorous shaking for one minute and then transferred to Wash II (340 mL water, 1 mL 20X SSC). The slide was dried by placing it in a 50 mL centrifuge tube with a Kimwipe in the bottom and centrifuged at 600 rpm for five minutes (Inada and Pleiss, 2010). The array was then scanned using an Olympus IX51 inverted laser scanning confocal microscope. The Cy3 and Cy5 channels were scanned sequentially with a 5 slice Z-stack to ensure even exposure across the array. The entire array was scanned using a 4X objective and the built-in stitching program with 90% overlap between images. Images were exported as 16-bit greyscale TIFF files for analysis.

cDNA synthesis for Dendrimer Labeled Microarray Analysis

cDNA synthesis reactions were set up to contain 10 µg RNA and 1 µL RT primer (1 pmole/µL), brought up to 11 µL with nuclease-free water. The RT primers were complementary to either the Cy3 or Cy5 capture sequence. The wild-type sample was annealed to the Cy3 primer and the mutant 18S sample was annealed to the Cy5 primer. The primers were annealed by heating the samples at 80°C for 10 minutes. The reactions were then transferred immediately to ice for 2-3 minutes. The cDNA reaction mix was prepared, mixed gently and kept on ice. The reaction mix consisted of 4 µL 5X Superscript II buffer, 2 µL 0.1M dithiothreitol/nuclease free water, 1 µL dNTPs (10 mM each), and 1 µL RT (Invitrogen Superscript II RT, 200 U/µL). Nine microliters of reaction mix were added to the 11 µL RNA-RT primer mix. The reaction was

gently mixed and incubated at 42°C for 2-3 hours. The reaction was stopped by adding 3.5 µL of 0.5 M NaOH/50 mM EDTA and incubating at 65°C for 15 minutes. The reaction was neutralized with 5 µL 1M Tris-HCl (pH 7.5). The two cDNA samples were combined and the empty tube rinsed with 73 µL TE buffer, which was combined with the cDNA samples. The samples were cleaned up using the cDNA cleanup protocol described previously.

Dye-Coupling and Array Hybridization for Dendrimer Labeled Microarray Analysis

To block the slide and prevent nonspecific hybridization, a 100 µL mixture of 3X SSC, 0.1% SDS and 0.1 mg/mL ssDNA was applied to the microarray slide and covered with a coverslip. The slide was incubated for 60 minutes. Following incubation, the coverslip was removed and the slide dipped in water. The slide was then spun dry in a 50 mL conical tube with a Kim-Wipe to collect drips by centrifuging for 5 minutes at 900 rpm. The 2X formamide-based hybridization buffer from the Genisphere Array 350 Kit was thawed and then incubated at 55°C for 10 minutes. The hybridization buffer was then mixed well and spun for one minute at 13,000 rpm. The cDNA samples were resuspened in 25 µL of water and 25 µL of the hybridization buffer was added. The samples were mixed gently, spun down, and incubated at 80°C for 10 minutes. The samples were kept at 42°C until ready to be put on the slide. The entire cDNA sample was applied to the slide and covered with a coverslip. The slide was placed in the hybridization chamber with 20 µL of 3X SSC on the label. The slide was then incubated at 37°C overnight.

The slide was removed from the hybridization chamber and transferred to Wash Solution I (2X SSC and 0.2% SDS) at room temperature and shaken gently to remove coverslip. The slide was then incubated at 55°C in Wash Solution II (2X SSC and 0.2% SDS) for 15 minutes.

The slide was then transferred to Wash Solution III (2X SSC) and incubated for 15 minutes at room temperature with periodic shaking. Finally, the slide was transferred to Wash Solution IV (0.2X SSC), incubated for 15 minutes at room temperature and dried by spinning for one minute at 500 rpm.

The 2X formamide hybridization buffer was thawed and incubated for 10 minutes at 55°C. The hybridization buffer was spun for one minute at 13,000 rpm. Both capture reagents were thawed, vortexed for three seconds and spun down. One hundred microliters of hybridization buffer was mixed with 1 µL antifade reagent from the Genisphere Kit. The hybridization mix was prepared and incubated for 10 minutes at 75°C. The hybridization mix consisted of 25 µL anti-fade-treated hybridization mixture, 20 µL DEPC-water, 2.5 µL Cy3 capture reagent and 2.5 µL Cy5 capture reagent. The mix was applied to the slide and covered with a coverslip. The slide was placed in the hybridization chamber with 20 µL 3X SSC on the label and incubated at 37°C overnight. Array washing was repeated as described previously and imaged using confocal microscope.

Microarray Analysis

Initial analysis of the microarray data was carried out by Diane Lee using MAGIC Tool (MicroArray Genome Imaging and Clustering), which was developed at Davidson College (Heyer et al., 2005). This was used to identify the top ten induced and repressed genes prior to normalization. Due to the low signal intensity of the data, normalization was performed prior to further analysis in R (Gentleman, 2005).

The software package Spot was used to obtain data from the microarray images (Beare, 2007). This program offered two methods of segmentation, which affect the way the image is

analyzed. The more traditional segmentation method is seeded region growing (SRG), but Spot also offers globally optimal geodesic active contours, or GOGAC, segmentation. GOGAC segmentation constrains the segmentation to a circular area, whereas SRG merely finds pixels that exceed a certain threshold, regardless of shape. When the images are of high contrast, the two methods will likely produce similar results (Beare, 2007). Because data was of low intensity, both segmentation methods were compared. We also used an alternative microarray gridding program, MASQOT-GUI, which enabled better edge detection of low-intensity spots (Bylesjö et al., 2006).

Data was normalized using two different methods: within array normalization and between array normalization. Within array normalization was performed using the program marray, and centers the log-ratios around zero, to account for dye or location bias (Yang, 2009). Dye bias can occur if the relative intensity of the dyes used to label wild-type and mutant samples differ. Location bias can occur if the samples are not evenly distributed on the microarray during hybridization, resulting in areas of higher signal intensity. Data was normalized using loess normalization (locally weighted scatterplot smoothing), which minimizes the bias caused by differences in spot location (Whitworth, 2010). Dye-swapped data, generated by switching the dyes used to tag the samples, was also compared. Traditionally, red dye is used for wild-type and green dye is used for mutant; in a dye-swap experiment, it is vice versa. Dye swapped data was subject to between-array normalization, which was performed using limma (Smyth, 2005). Limma, a program within R, served many functions, including normalization of raw data and statistical analysis of differential gene expression. Between-array normalization ensures that the distribution of log-ratio values is comparable between microarrays (Gentleman, 2005). Limma also performed a background correction that changes the distribution

of the intensity values based on a normal distribution of foreground intensities and an exponential distribution of background intensities.

Limma was used to determine which genes are differentially expressed by controlling for false discovery rates and calculating the probability that a gene is differentially expressed using Bayesian statistics (Gentleman, 2005). However, comparisons between the two dye-swapped arrays may not reveal all genes of interest due to differences between the swapped and unswapped arrays. Therefore replicates within a single array were also examined, which should have similar values.

## Results and Discussion

### Overview of Experimental Trajectory

Many of the mechanistic details of NRD remain to be elucidated. A more detailed understanding of the pathway will provide insight into the relationship between NRD and other RNA degradation pathways as well as the biological relevance of NRD. To gain insight into novel genes involved in NRD, we used microarray analysis to examine the global changes in gene expression that take place when NRD is activated. Wild-type yeast cells were transformed with galactose-inducible plasmids containing defective rRNAs to activate NRD. Following plasmid activation upon transfer to galactose media, total RNA was isolated from the cells. Plasmid-derived ribosomal RNA was analyzed using RT-qPCR to determine activation of the NRD pathway and degradation of defective rRNAs. The mRNA population, corresponding to transcribed genes, were reverse transcribed to cDNA and fluorescently labeled using the Cy dyes. These samples were hybridized to the microarrays. Microarrays were then imaged and analyzed to determine overall changes in gene expression between cells with wild-type rRNAs and those with NRD substrates. Due to issues with low signal, we also attempted a similar trajectory with the temperature sensitive NOY504 strain.

### RT-qPCR Analysis of BY4741

Following transformation of the BY4741 strain with WT, 18S, 25S and DM plasmids, RNA integrity was determined by agarose gel electrophoresis (Figure 11). RNA was then analyzed by RT-qPCR. RT-qPCR results were analyzed by converting $C_T$ values to amount of RNA in nanograms, normalized to the amount of uracil template. Values are reported as ratio to wild-type (Table 4).

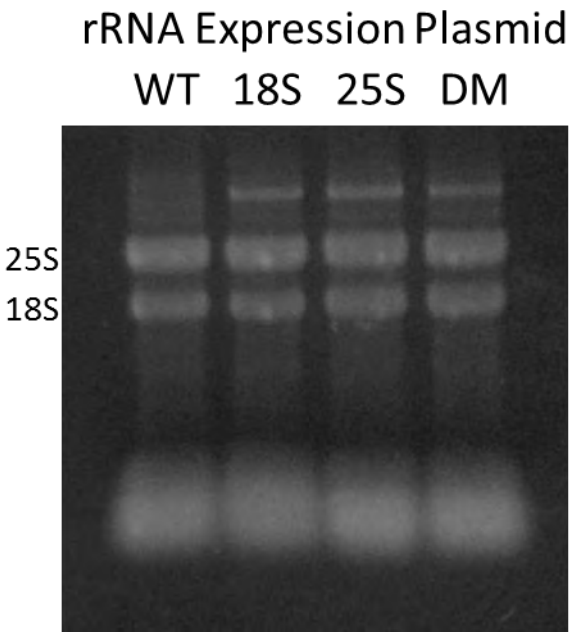


**Figure 11: Agarose gel of BY4741 transformants.** 25S and 18S rRNAs designated with labels on left of figure. Labels above lanes indicate which pSC1 plasmid is present. 1% agarose gel stained with ethidium bromide.

**Table 4: RT-qPCR analysis of BY4741 transformants.**

| | | Plasmid | | | |
|---|---|---|---|---|---|
| | | WT[1] | 18S | 25S | DM |
| Primer | 18S | 1 | 0.39 ± 0.03 | 0.28 ± 0.02 | 0.018 ± 0.006 |
| | 25S | 1 | 2.1 ± 0.1 | 0.172 ± 0.006 | 0.29 ± 0.02 |

[1] All values normalized to wild-type. Error represents range of experimental values.

The low relative amounts of plasmid-derived 18S and 25S rRNA in the double-mutant and single mutant samples confirms that NRD is actively degrading these substrates, consistent with previous results (Table 4). The 18S rRNA levels are somewhat low in the mutant 25S transformant, but are relatively higher than the 25S rRNA levels. The 25S rRNA levels are also high in the 18S mutant. These types of variability are seen during RT-qPCR analysis and may represent random effects not taken into account during normalization.

RT-qPCR Analysis of NOY504 Strain

Use of the NOY504 strain required a more complicated procedure. When the strain is grown at 37°C, endogenous rRNA expression is shut off. To ensure viability, the NOY504 strain must also be transformed with an additional plasmid encoding functional rRNA. We used the pWL155/pWL160 plasmid, a galactose-inducible plasmid containing a tryptophan marker and functional 18S and 25S rRNA. We did a double transformation of the pWL160 plasmid with each of the pSC1 plasmids. However, the pWL160 plasmid contains the same sequence tags for RT-qPCR as the pSC1 plasmid, so to prevent this from interfering with our results we also transformed the pWL155 plasmid with each of the pSC1 plasmids.

RNA was isolated from NOY504 transformed with the pSC1 plasmids and NOY504 transformed with pWL160/pWL155 and the pSC1 plasmids. The isolated RNA was run on an agarose gel to determine the integrity of the isolated RNA, which was determined to be suitable for cDNA synthesis in both cases (Figure 12).

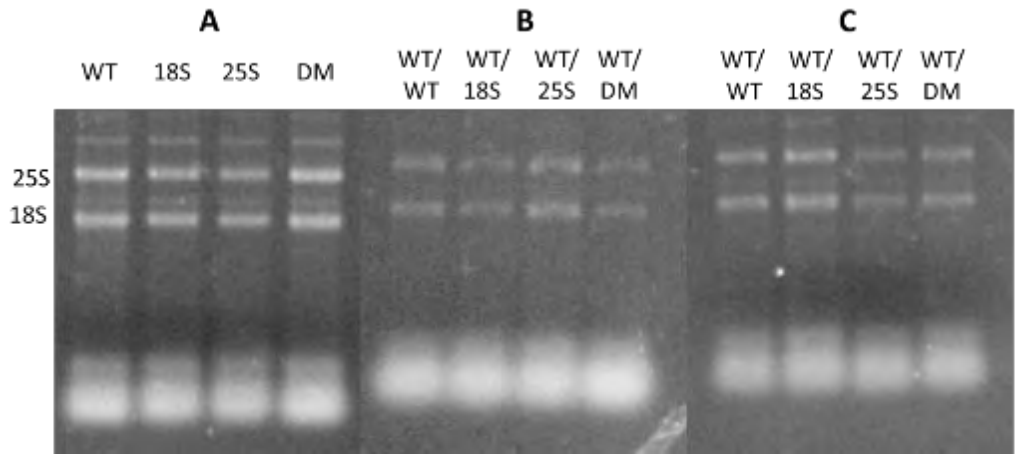


**Figure 12: Agarose gel of RNA isolated from NOY504 strain.** 25S and 18S rRNAs designated with labels on left of figure. 1% agarose gel stained with ethidium bromide. (A) NOY504 transformed with the four pSC1 plasmids. (B) NOY504 transformed with pWL160 and the four pSC1 plasmids. (C) NOY504 transformed with pWL155 and the four pSC1 plasmids.

In order for the NOY504 strain to be a good candidate for future microarray experiments, we had to verify using RT-qPCR that NRD is acting similarly in NOY504 and BY4741. Analysis of NOY504 transformed with the pSC1 plasmids yielded results that did not match our expected results (Table 5). In NOY504::pSC1-25S, we expect 25S rRNA levels to be down and 18S rRNA levels to remain stable in comparison. Instead we see that both 18S and 25S rRNA levels are down, with 18S rRNA levels lower than 25S. This experiment was repeated to verify these results, and again we did not see strong evidence for typical NRD.

**Table 5: RT-qPCR Analysis of NOY504 transformed with pSC1 plasmids.**

| | | Plasmid | | | |
|---|---|---|---|---|---|
| | | NOY504::pSC1-WT[1] | NOY504::pSC1-18S | NOY504::pSC1-25S | NOY504::pSC1-DM |
| **Primer** | 18S | 1 | 0.18 ± 0.02 | 0.187 ± 0.003 | 0.34 ± 0.02 |
| | 25S | 1 | 0.32 ± 0.04 | 0.22 ± 0.04 | 0.15 ± 0.03 |

[1] All values normalized to wild-type. Error represents range of experimental values.

RT-qPCR analysis of NOY504 with pWL160 and pSC1 plasmids generated some unexpected results as well (Table 6). One explanation may be the overlap in sequence tags on the pWL160 plasmid with the pSC1 plasmids, meaning that RT-qPCR amplifies rRNA derived from both plasmids, while we are only interested in levels of rRNA derived from the pSC1 plasmids. To resolve this problem, we looked at RT-qPCR analysis of NOY504 with pWL155 and pSC1 plasmids, since the pWL160 plasmid does not have this overlap of sequence tags.

**Table 6: RT-qPCR Analysis of NOY504 transformed with pWL160 and pSC1 plasmids.**

| | | Plasmid | | | |
|---|---|---|---|---|---|
| | | NOY504::pWL160 ::pSC1-WT[1] | NOY504::pWL160 ::pSC1-18S | NOY504::pWL160 ::pSC1-25S | NOY504::pWL160 ::pSC1-DM |
| **Primer** | 18S | 1 | 1.5 ± 0.2 | 0.94 ± 0.07 | 1.4 ± 0.1 |
| | 25S | 1 | 0.57 ± 0.03 | 0.7 ± 0.1 | 0.24 ± 0.03 |

[1] All values normalized to wild-type. Error represents range of experimental values.

Analysis of the NOY504 strain transformed with the pWL155 and pSC1 plasmids generated results that resemble those expected when NRD is active (Table 7). In NOY504::pWL155::pSC1-18S, the levels of 18S rRNA derived from the pSC1 plasmid are down, indicating that 18S NRD is activated, while 25S rRNA levels are relatively stable. The 25S rRNA levels are somewhat lower than wild-type, which may indicate concurrent degradation of 25S rRNA during 18S NRD, which is anticipated if the quality control mechanism is unable to distinguish which subunit is defective. For NOY504::pWL155::pSC1-25S, 25S rRNA levels are low while 18S rRNA levels are stable, indicating that 25S NRD is actively degrading defective 25S rRNA. In NOY504::pWL155::pSC1-DM, both levels of 18S and 25S rRNA are down, indicating that both forms of NRD are active in this strain. These results are promising, as they demonstrate that the NOY504 strain shows expected NRD activity at 25°C.

**Table 7: RT-qPCR analysis of NOY504 transformed with pWL155 and pSC1 plasmids.**

| | | Plasmid | | | |
|---|---|---|---|---|---|
| | | NOY504::pWL155 ::pSC1-WT[1] | NOY504::pWL155 ::pSC1-18S | NOY504::pWL155 ::pSC1-25S | NOY504::pWL155 ::pSC1-DM |
| **Primer** | 18S | 1 | 0.177 ± 0.02 | 1.4 ± 0.2 | 0.11 ± 0.03 |
| | 25S | 1 | 0.64 ± 0.08 | 0.100 ± 0.007 | 0.17 ± 0.02 |

[1] All values normalized to wild-type. Error represents range of experimental values.

Phenotypic Analysis

For a qualitative measure of plasmid expression and temperature sensitivity in the NOY504 strain, we performed phenotypic analysis. For analysis of the NOY504 strain containing just the pSC1 plasmids, galactose cultures were diluted to the same O.D. before making a dilution series of six five-fold dilutions, which was duplicated on the bottom half of

each plate. This dilution series was plated on glucose and galactose URA$^-$ plates in duplicate using a frogger. Plates were incubated in three temperature conditions: 25°C, 30°C, and 37°C. The results from this analysis follow our anticipated results (Figure 13). At 25°C, all transformants grow on both glucose and galactose, due to the excess of endogenous rRNAs.

Growth is less robust on galactose, which is to be expected since glucose is the preferred sugar. At 30°C, the transformants are still able to grow on glucose plates due to the presence of endogenous rRNAs, though at a lower level. This distinction is seen on the galactose plates, where differences between wild-type and mutant plasmids become more obvious due to increased reliance on plasmid-derived rRNA. At 37°C, none of the transformants are able to grow on glucose due to the shut-off of endogenous rRNA and restriction of plasmid expression on glucose media. On galactose, only the transformant with the wild-type plasmid is able to grow because all plasmid derived rRNAs are degraded by NRD in the other transformants.

For analysis of the NOY504 strain containing the pWL160/pWL155 and pSC1 plasmids, galactose cultures were diluted to the same O.D. before making a dilution series of four ten-fold dilutions, which was duplicated on the right half of each plate. This dilution series was frogged onto glucose and galactose URA$^-$ plates in duplicate, which were incubated in three temperature conditions: 25°C, 30°C, and 37°C. The results from this analysis follow our anticipated results (Figure 14). At 25°C, all transformants grow on both glucose and galactose, due to the excess of endogenous rRNAs. At 30°C, the transformants are still able to grow on glucose plates due to the presence of endogenous rRNAs, though at a lower level. On galactose plates, we see more robust growth due to the expression of the wild-type pWL160 or pWL155 in all strains. At 37°C, none of the transformants are able to grow on glucose due to the shut-off of endogenous rRNA

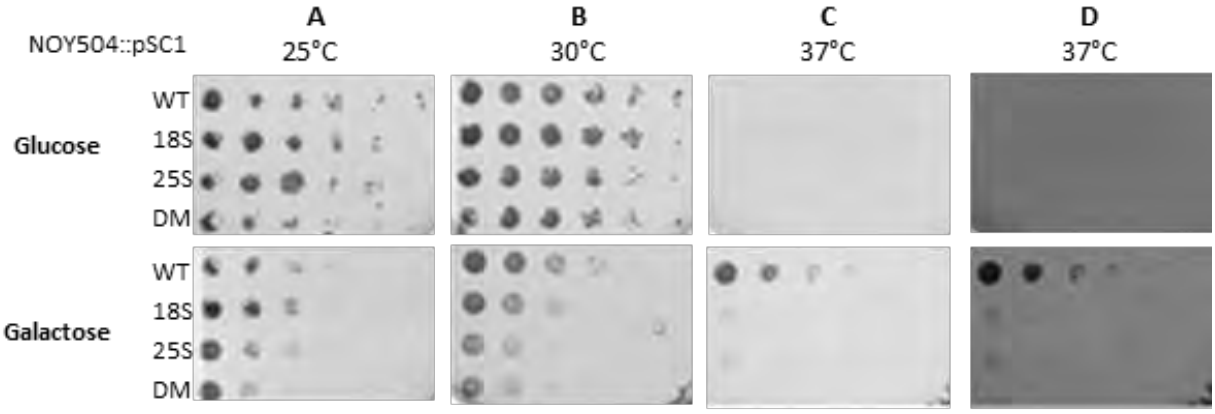


**Figure 13: Phenotypic analysis of NOY504::pSC1.** NOY504 transformed with four pSC1 plasmids (WT,18S, 25S and DM). Six 5-fold dilutions were made and incubated at the given temperature and medium until colonies were visible. One of four replicates shown.
(A) NOY504::pSC1 incubated at 25°C on URA$^-$ glucose (top) and URA$^-$ galactose (bottom).
(B) NOY504::pSC1 incubated at 30°C on URA$^-$ glucose (top) and URA$^-$ galactose (bottom).
(C) NOY504::pSC1 incubated at 37°C on URA$^-$ glucose (top) and URA$^-$ galactose (bottom).
(D) Darker exposure of panel C.

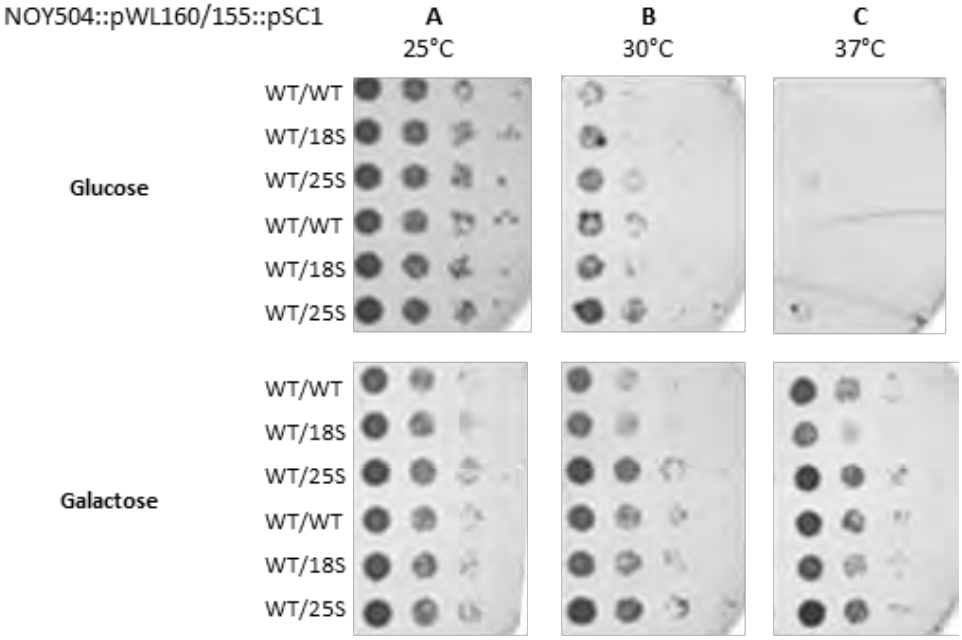


**Figure 14: Phenotypic analysis of NOY504::pWL160/155:pSC1.** The top three cultures on each panel are transformed with the pWL160 plasmid and pSC1-WT, pSC1-18S and pSC1-25S, in that order. The bottom three cultures on each panel are transformed with the pWL155 plasmid and the pSC1-WT, pSC1-18S and pSC1-25S, in that order. One of four replicates shown.
(A) NOY504::pWL160/155::pSC1 incubated at 25°C on URA$^-$ glucose (top) and URA$^-$ galactose (bottom). (B) NOY504::pWL160/pWL155::pSC1 incubated at 30°C on URA$^-$ glucose (top) and URA$^-$ galactose (bottom). (C) NOY504::pWL160/pWL155::pSC1 incubated at 37°C on URA$^-$ glucose (top) and URA$^-$ galactose (bottom).

and restriction of plasmid expression on glucose media. On galactose, all transformants with the wild-type plasmid are able to grow since all defective plasmid derived rRNAs are degraded by NRD.

Although the NOY504 strain transformed with the pSC1 and pWL155 plasmids showed some promise for future microarray experiments, due to inconsistencies with the RT-qPCR results and difficulty of transformation and growth of the strain, we decided to return to BY4741 for future microarray experiments.

DNA Microarrays

The initial microarray experiment carried out by Diane Lee involved the use of fluorescent dendrimers, small molecules with multiple fluorescent molecules attached that were used to label the cDNA samples upon hybridization to the microarray (Genisphere). This experiment compared cells transformed with the wild-type rRNA expression plasmid to those transformed with either the mutant 18S or 25S rRNA expression plasmid. Each of the microarray experiments was also performed as a dye-swap, in which the dyes used to label the wild-type and experimental sample were switched. Due to low signal intensity, we decided to switch to a more traditional method of cDNA labeling, which involves incorporation of aminoallyl-dUTP during cDNA synthesis. This modified nucleotide is then directly coupled to fluorescent dyes, either Cy3 or Cy5. By convention, the experimental sample is labeled with Cy5 and the control sample is labeled with Cy3. In this case, a red spot on the microarray corresponds to an overexpressed gene in the experimental sample and a green spot corresponds to an underexpressed gene. In the dye-swap experiments, the labeling is switched to account for any dye bias during the experiment. The microarray experiment performed in this study

compared cells transformed with the wild-type rRNA expression plasmid to those transformed with the double-mutant rRNA expression plasmid. A dye swap experiment and two biological replicate experiments (for swapped and unswapped) were also performed for a total of four microarrays. Each microarray contains two identical copies of the DNA probes for within array replicates, giving us eight total replicates for each DNA spot.

An additional modification we made during this experiment was the imaging of the microarrays on site using a confocal microscope. Typically the microarrays are shipped off to be imaged, which results in signal loss due to the time required for shipping. Our initial experiments did not show signal on the confocal, so modifications and troubleshooting of the cDNA synthesis and coupling reactions was necessary. By remaking the aa-dUTP + dNTP mixture and switching to the Clontech SMART MMLV RT, we were able to increase the yield of cDNA synthesis. Further troubleshooting of dye coupling conditions revealed that the optimal conditions for dye-coupling were at 60°C for one hour with recent suspension of the dye in DMSO (data not shown). Additional troubleshooting with the confocal revealed that the Cy3 and Cy5 channels had to be scanned sequentially in order to separate the signals, which have somewhat overlapping emission spectra. Confocal scanning of microarrays was ultimately successful in generating microarray image for data analysis (Figure 15).

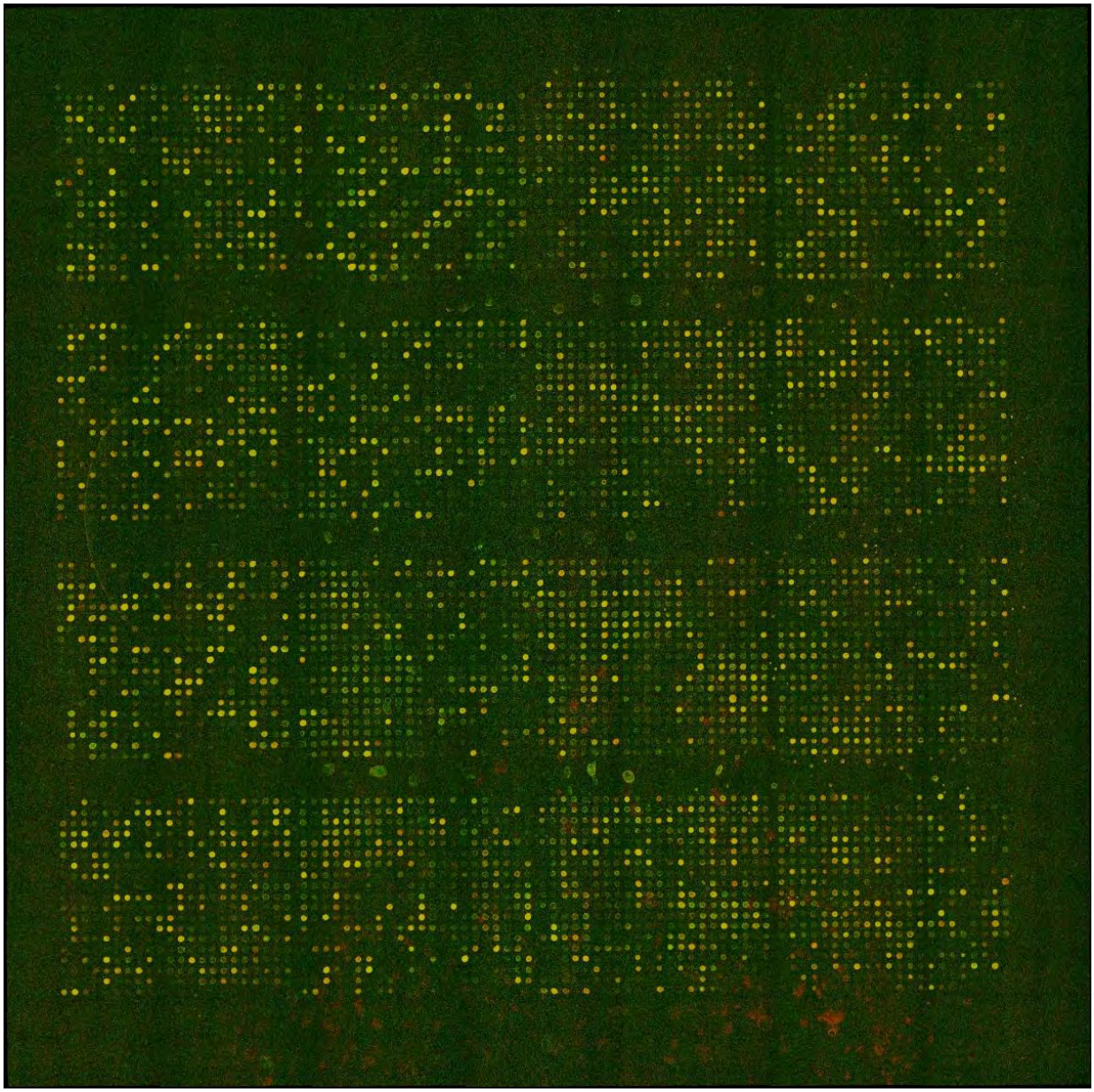

**Figure 15: Microarray image generated with confocal microscopy**. This image represents one half of the microarray, where the second half contains replicates of the DNA spots. In this array, the WT sample is labeled with Cy3 dye and the experimental sample is labeled with Cy5 dye.

Microarray Data Analysis

Initially, we analyzed previous microarray data using R, the statistical computing program. The microarray data is presented as an MA Plot, which compares the log base two ratio of the dye intensities (M) to the average intensity of the dye (A) (Figure 16). In this analysis, positive log ratio values (M values) indicate induction of genes. Prior to normalization, the dye bias is evident, especially in the low intensity data (Figure 16A). Free of bias, the data would be centered at zero, which is what the normalization process tries to replicate (Figure 16B).

This type of within array normalization does not take into account the differences that occur between different arrays, such as between the separate swapped and unswapped arrays. Normalization between these arrays adjusts the distribution of intensity values because on some arrays red or green fluorescence may dominate (Figure 17A). After between array normalization, the distribution of intensities between arrays is more comparable, which aids the statistical comparison of genes using data from different arrays (see Figure 17B).

The resulting MA Plot from the between array normalization (Figure 18) shows that genes with significant intensity and large M values are conserved, while those with low intensity are concentrated at zero. This plot also differs from the marray normalized one due to the background correction performed on limma, which positively shifted our intensity values, since our raw intensity values were so low to begin with. Due to the differences between these two normalization techniques, both were considered when identifying genes with significant differential expression.

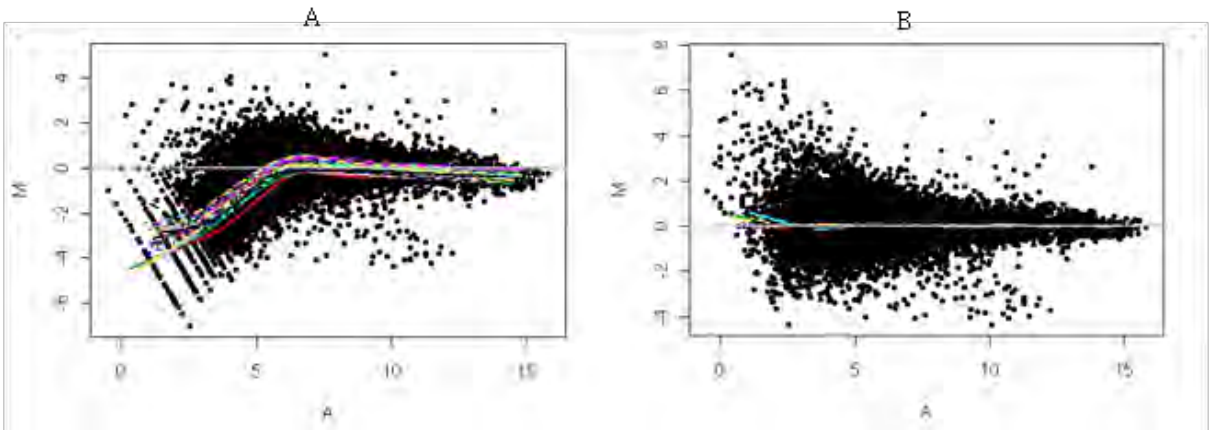


**Figure 16: Raw and normalized 18S swapped microarray data.** (A) Raw data. (B) Normalized data. Microarray signal was quantified using seeded region growing segmentation and normalized using print-tip loess normalization in marray. M values correspond to the $\log_2$ ratio of green to red intensity ($M = \log_2 G - \log_2 R$). A values correspond to the intensity of the signal ($A = \frac{1}{2}(\log_2 G + \log_2 R)$).

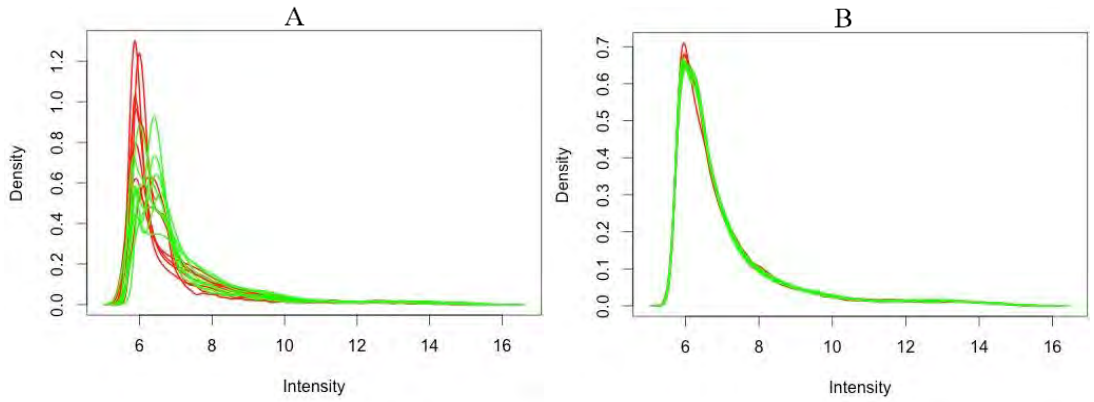


**Figure 17: Raw and normalized distribution of red and green intensities across all arrays.** (A) Data from all arrays prior to between array normalization. (B) Data normalized using limma. Red lines correspond to the distribution of red dye intensity in one array, and green lines correspond to the distribution of green dye intensity. Intensity corresponds to the intensity of the signal ($A = 1/2 \times (\log_2 G + \log_2 R)$).

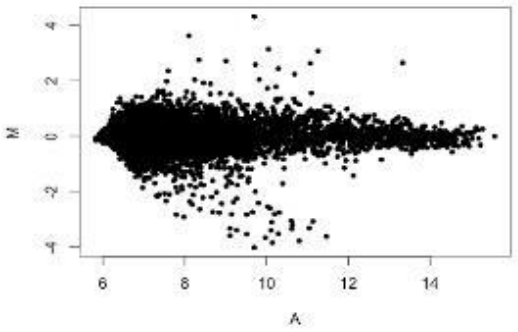


**Figure 18: Normalized 18S swapped microarray data.** This data was analyzed using seeded region growing segmentation technique. It was background corrected in limma and normalized, both with within array and between array normalization. M corresponds to the $\log_2$ ratio of green to red intensity ($M=\log_2 G - \log_2 R$). A corresponds to the intensity of the signal ($A= 1/2 \times (\log_2 G + \log_2 R)$).

R also allowed us to compare between arrays to identify differentially expressed genes using Bayesian probability. However, differences between the swapped and unswapped array did not yield significant probabilities that any genes were differentially expressed.

We decided to look at within array replicates as well, which should have a better correlation since they come from the same sample. By plotting the replicates, we were able to focus on genes within two standard deviations of the line of symmetry, which is where all the genes would fall if they were perfectly replicated (Figures 19). Differences between marray normalized data (Figure 19A) and limma normalized data (Figure 19B) verified the use of these two normalization techniques, as they yielded different results.

Genes that fit the criteria of falling within two standard deviations and with an absolute value of M over 1 after analysis in marray are listed in Table 8. An interesting gene from the 18S and 25S data is TOF2, which is involved in rDNA silencing. A number of genes encoding ribosomal proteins may be induced by 25S NRD, perhaps indicating the need for increased production of ribosomal proteins following degradation by NRD. We also see that ubiquitin may be upregulated by 25S NRD, consistent with the working model in which NRD substrates are tagged with ubiquitin for degradation.

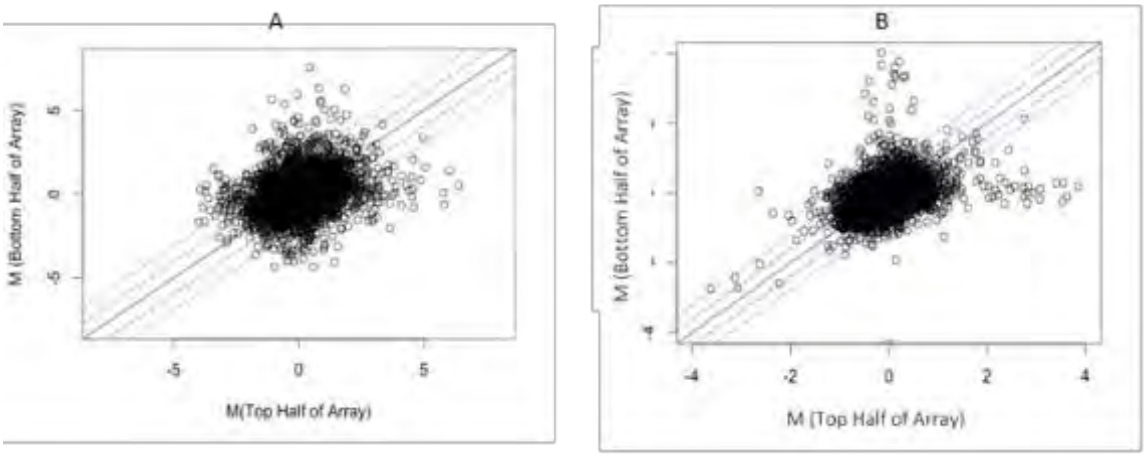


**Figure 19: Replicate plot of 18S swapped data.** (A) Data analyzed using seeded region growing segmentation technique and normalized using within array normalization on marray. (B) Data analyzed using seeded region growing segmentation technique and normalized using within array normalization and between array normalization on limma. The solid line corresponds to the line of symmetry, where the points would fall if they were perfect replicates. The blue dashed lines correspond to one standard deviation from the line of symmetry. The red dashed lines correspond to two standard deviations from the line of symmetry.

**Table 8: Partial list of genes identified by microarray analysis**[i]

| 25S Microarray | | | |
|---|---|---|---|
| **Gene** | **Function** | **$Log_2$ Expression Ratio (M)** | **Spot Intensity Value (A)** |
| *RPP1A* | Ribosomal stalk protein | 2.6106<br>2.5380 | 12.1167<br>11.6670 |
| *RPL2A* | Ribosomal 60S subunit protein | 2.7338<br>3.2081 | 8.4299<br>5.6174 |
| *RPL30* | Ribosomal 60S subunit protein | 2.5477<br>3.6151 | 11.3074<br>7.2778 |
| *TOF2* | Involved in rDNA silencing | 2.2209<br>4.1903 | 8.6167<br>8.4543 |
| *UBI4* | Ubiquitin; marks proteins for selective degradation | 2.8253<br>2.0580 | 6.5894<br>5.2376 |
| *NOP13* | Nucleolar protein found in preribosomal complexes | 2.9885<br>2.4717 | 6.2478<br>6.3627 |
| *SSA4* | Heat shock protein | -3.3786<br>-3.0697 | 6.7262<br>6.8641 |
| *YJR056C* | Unknown function, distribution to the nucleus increases upon DNA replication stress | -2.8724<br>-3.0355 | 10.5181<br>9.7492 |
| **18S Microarray** | | | |
| *GPN3* | GTPase with a role in biogenesis of RNA pol II and polIII | 3.4524<br>4.7870 | 9.0959<br>8.3739 |
| *TOF2* | Involved in rDNA silencing | 2.8873<br>5.1451 | 7.4227<br>6.6287 |
| *RPP2A* | Component of the ribosomal stalk | -3.8276<br>-3.5959 | 12.1674<br>11.5613 |
| *UBI4* | Ubiquitin; marks proteins for selective degradation | -2.2763<br>-2.4467 | 8.0076<br>7.3274 |

[i] Red indicates induced genes, green repressed genes

Similar normalization and analysis techniques were used for the microarray data collected using confocal microscopy. Due to issues with array gridding and segmentation of low intensity spots in Spot, segmentation was carried out using MASQOT-GUI instead (Bylesjö et al., 2006). This program gave a more accurate distinction between foreground and background of low intensity spots. Data was initially processed using loess normalization in marray (Figure 20), but large differences in dye distribution between the arrays made additional normalization in limma necessary. The raw distribution of red and green pixel intensities in the raw data show these large differences (Figure 21A). Following loess normalization and between array normalization, the distributions were much more even (Figure 21B,C). Limma also performs a background subtraction called normexp that uses models signal pixel intensities as a normal distribution and background pixel intensities as an exponential distribution (Figure 22). This type of normalization has been described as the best background correction method for 2-color microarray data (Ritchie et al., 2007). We also analyzed data without any background correction (Figure 23).

Replicate plots following normalization indicate reproducibility of replicates, including within array replicates (Figure 24A), biological replicates (Figure 24B) and dye swap replicates (Figure 24C). These plots indicate how accurate each set of replicates are and may be used in additional data analysis or quality control.

Following normalization, microarray data was analyzed using Bayesian probability testing in limma to determine genes that were differentially expressed across all arrays. Data was also analyzed using hierarchical clustering in Cluster 3.0 and Java Treeview. First we examined the expression changes of genes previously implicated in the NRD pathway (Figure 25). We expect that factors involved in NRD may show increased transcription in response to

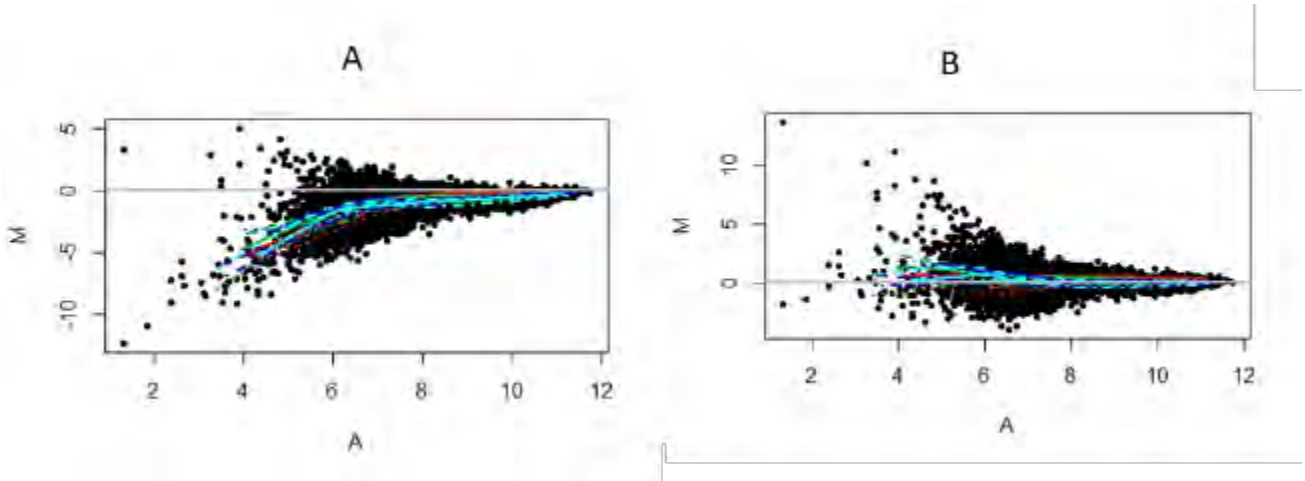


**Figure 20: MA plots of raw and normalized microarray data.** Shown is unswapped microarray data comparing gene expression of cells transformed with the pSC1-WT plasmid versus pSC1-DM plasmid. Data was analyzed using mean foreground and background intensities and normalized using loess normalization in marray. Colored lines indicate mean intensities of each block. The grey line indicates an M value of zero.

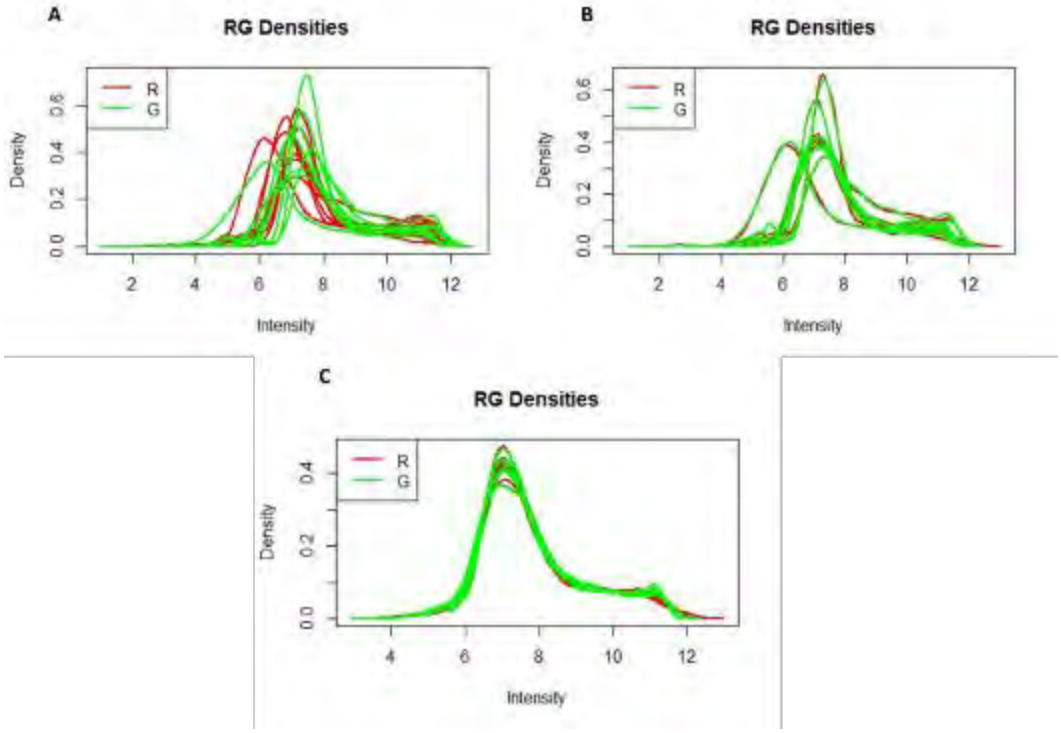


**Figure 21: Distributions of red and green intensities during normalization in limma.** Data was analyzed by using mean foreground and background intensities and was subject to normexp background subtraction in limma. (A) Raw red and green intensity distributions. (B) Red and green intensity distributions following loess normalization. (C) Red and green intensity distributions following between array normalization.

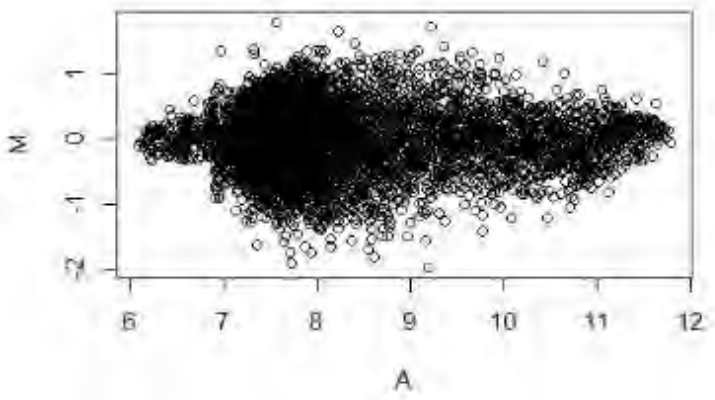


**Figure 22: MA plot of microarray data following normalization in limma.** Shown is unswapped microarray data comparing gene expression of cells transformed with the pSC1-WT plasmid versus pSC1-DM plasmid. Data was analyzed using mean foreground and background intensities and normalized using loess normalization and normexp background subtraction in limma.

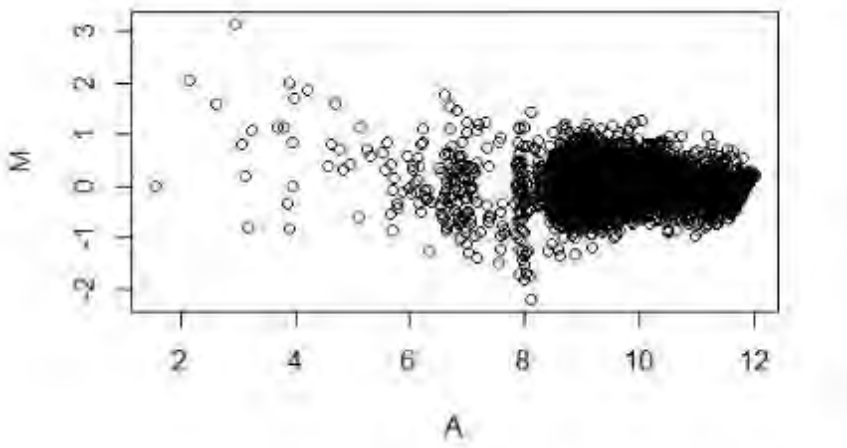


**Figure 23: MA plot of microarray data following normalization in limma without background correction.** Shown is unswapped microarray data comparing gene expression of cells transformed with the pSC1-WT plasmid versus pSC1-DM plasmid. Data was analyzed using mean foreground and background intensities and normalized using loess normalization and between array normalization.

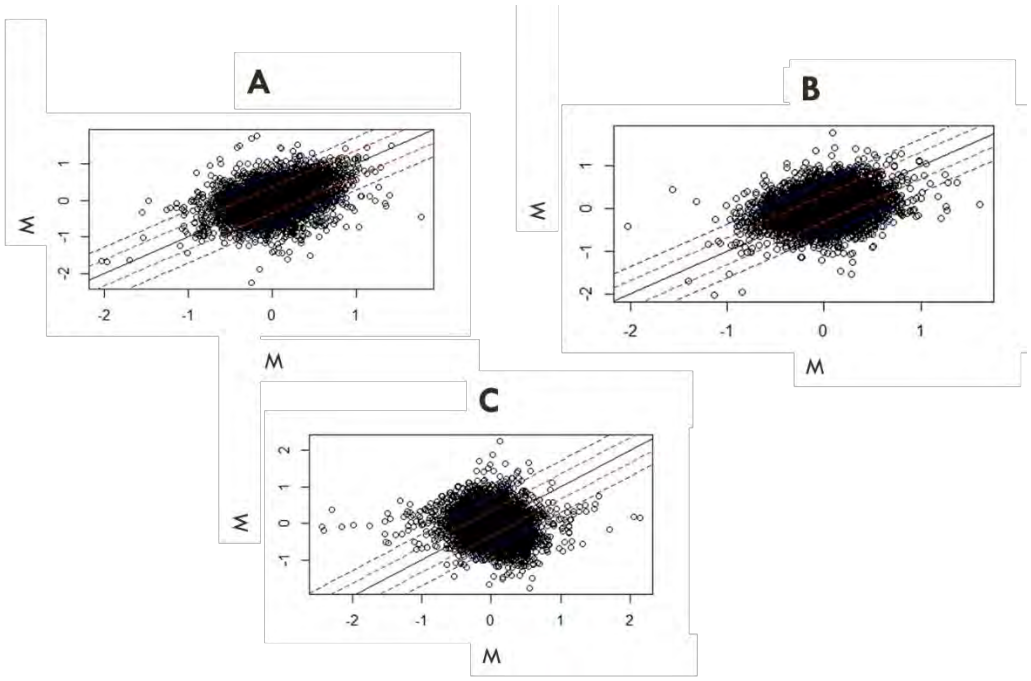


**Figure 24: Replicate plots following normalization.** Data was normalized using background subtraction, normexp background correction, loess smoothing and between array normalization. (A) Within-array replicates. (B) Biological replicates. (C) Dye swap replicates.

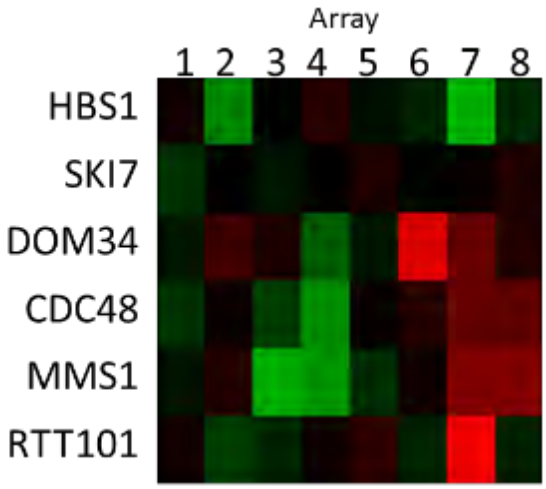


**Figure 25: Cluster diagram of known genes in NRD.** Data was subject to background subtraction, loess normalization and within array normalization. Green blocks correspond to negative fold change/decreased expression and red blocks correspond to positive fold change/increased expression. Arrays 1 and 2, 3 and 4, etc. are within array replicates. Arrays 1 and 3, 2 and 4, etc. are biological replicates. Arrays 5-8 are dye swap replicates of 1-4. Clustering performed in Cluster 3.0 and Java Treeview.

the presence of NRD substrates in the double-mutant transformant, where an increase in transcription would show up as red for the unswapped arrays and green for the swapped arrays. We see that the majority of the genes involved in NRD show inconsistencies across arrays. Dom34 expression appears to be upregulated across most of the arrays, which is what we would expect. However, Hbs1 expression appears downregulated across most of the arrays, which is the opposite of what we would anticipate.

We also examined expression changes of genes identified in the previous microarray experiment (Figure 26). Analysis of previously identified genes also revealed mixed results. YJR056C, Rpl2A, Tof2 and Gpn3 were induced in the previous microarray experiment and show a similar pattern of expression in this experiment as well. Rpp2A was found to be repressed when 18S NRD was activated, and we saw a similar result in the double-mutant experiment as well. Rpl30 and Rpp1A showed increased expression when 25S NRD was activated, but here show consistent downregulation in the double-mutant array. The remaining genes showed inconsistencies across the arrays.

Differential expression analysis in limma was used for preliminary analysis to determine genes of interest (Table 9). A recurring theme was that genes upregulated by DNA replication stress also seem to be induced by NRD. Other genes of interest include OTU1, whose protein product binds known NRD factor Cdc48p. This gene was found to be downregulated when NRD substrates are present and encodes a deubiquitylation enzyme. Since ubiquitylation of ribosomal proteins is necessary for 25S NRD, downregulation of Otu1p may enhance 25S NRD. Other genes whose expression is repressed include other RNA processing factors NSA2 and JIP5. JIP5 is another interesting finding as it is required for 25S subunit biogenesis and interacts with proteins involved in RNA processing, but its precise role has not yet been uncovered.

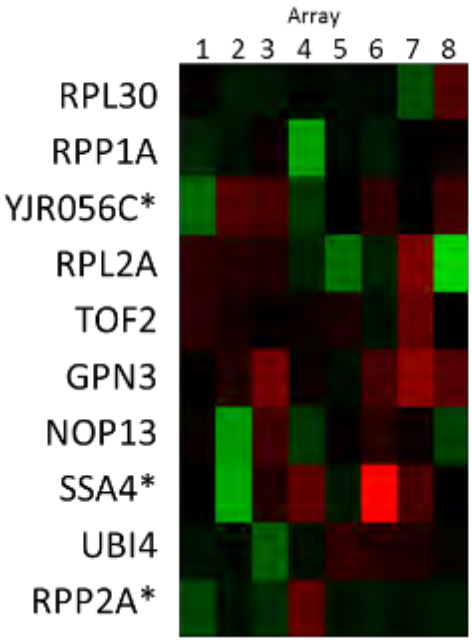


**Figure 26: Cluster diagram of previously identified genes.** Data was subject to background subtraction, loess normalization and within array normalization. Green blocks correspond to negative fold change/decreased expression and red blocks correspond to positive fold change/increased expression. Starred genes were found to be repressed in earlier analysis. Arrays 1 and 2, 3 and 4, etc. are within array replicates. Arrays 1 and 3, 2 and 4, etc. are biological replicates. Arrays 5-8 are dye swap replicates of 1-4. Clustering performed in Cluster 3.0 and Java Treeview.

**Table 9: Differentially expressed genes.**[ii]

| Gene | Function | $Log_2$ Expression Ratio (M) | Spot Intensity Value (A) |
|---|---|---|---|
| *ADE13* | Adenylosuccinate lyase; involved in 'de novo' purine nucleotide biosynthesis | 0.6710 | 9.1998 |
| *NSA2* | Protein found in 66S pre-ribosomal particles processing the 27S pre-rRNA | -0.5799 | 7.8551 |
| *JIP5* | Required for biogenesis of the large ribosomal subunit; interacts with proteins involved in RNA processing, ribosome biogenesis, ubiquitination and demethylation | -0.6188 | 9.1607 |
| *SUV3* | ATP-dependent RNA helicase found in mitochondrial degradosome along with the RNase Dss1p; the degradosome associates with the ribosome and mediates RNA turnover | -0.5755 | 7.9034 |
| *OTU1* | Deubiquitylation enzyme that binds to the chaperone-ATPase Cdc48p; may contribute to regulation of protein degradation by deubiquitylating substrates that have been ubiquitylated by Ufd2p | -1.1595 | 6.2144 |

[ii] Red indicates induced genes, green repressed genes

## Conclusion

DNA microarrays allow for the assessment of global gene expression changes taking place in an experimental system. This type of analysis has the potential to uncover novel factors involved in NRD. Identification of essential factors involved in NRD not only reveals important mechanistic details, but also may also relate the pathway to existing RNA degradation mechanisms. In this project we sought to analyze previously collected microarray data as well as improve the signal in a follow-up microarray experiment by altering the strain used, the method of dye incorporation and the method of microarray imaging.

Although the use of the NOY504 strain for microarray analysis showed some promise, issues with transformations, growing times and proper activation of NRD made the strain unsuitable for our experiments. However, the use of the dual plasmid system was successful and this strain may be used in the future for additional experiments. In addition, we were able to successfully scan our microarrays on campus using confocal microscopy. This offers us the ability to scan microarrays and other fluorescently-labeled experiments on site without having to ship them to another location, during which time dye degradation can occur. This technique can still be improved to allow for higher intensity signal across the sample without saturating bright spots, which was an issue during this analysis.

The results obtained from the microarray analysis are still being analyzed to determine differentially expressed genes. We plan on using the program SAM (Significance Analysis of Microarrays) to mine more relevant data on the NRD pathway. Initial data analysis shows promise in that genes that fit into the NRD pathway framework seem to be affected by activation of the pathway. Genes that seem to be upregulated by activation of NRD include ribosomal protein genes, DNA replication stress response genes and rDNA silencing genes. Additionally,

we observed upregulation of ubiquitin following activation of 25S NRD, consist with observation of ubiquitylation as a tagging method for 25S NRD substrates. We also observed downregulation of Otu1p, a deubiquitylation enzyme. Additionally, downregulation of other known RNA processing and degradation factors was also observed in initial analysis. Once genes of interest have been determined with suitable confidence, we plan to test them directly for involvement in NRD by transforming knockout strains with NRD substrate plasmids and examining NRD activity via RT-qPCR. If these genes encode factors required for NRD, we expect that NRD substrates will not be degraded as efficiently in these knockout strains. These methods are well developed in our lab and will hopefully uncover additional details about the NRD pathway.

## Appendix

We performed additional data analysis of microarray data. After examining replicate plots, we found a low degree of correlation between dye swap replicates. Therefore, data analysis for the two sets of dye swap replicates was performed separately. For the first set of arrays corresponding to those with the wild-type sample labeled with Cy3 and the experimental sample labeled with Cy5, data was normalized using normexp background correction in limma (Figure 27B) and loess normalization (Figure 27C). Low signal spots were removed from data by calculating the average intensity value (A value) of the blank spots on each array and filtering out spots with intensities falling below this threshold (Figure 27D). Arrays were then normalized using between array quantile normalization (see Figure 21 for example, data). Plots of array replicates and biological replicates display correlation between the two sets of replicates (Figure 28). Correlation between replicates was also determined using the Pearson correlation coefficient (Figure 29). The Pearson correlation coefficient is a measure of the linear correlation between two variables, with a value of 1 being a purely positive correlation, 0 no correlation, and -1 a purely negative correlation. These values indicate that agreement between within-array replicates was higher than agreement between biological replicates (Figure 29). Similar analysis was performed for the second set of arrays, however only global median normalization and between array quantile normalization was performed, which maximized agreement between replicates in this case. Low intensity spots were filtered out as described before. Correlation between replicates was determined using the Pearson correlation metric as before (Figure 30).

Data from arrays was grouped to identify genes showing uniform expression using k-means clustering. As opposed to hierarchical clustering, which focuses on local relationships, k-

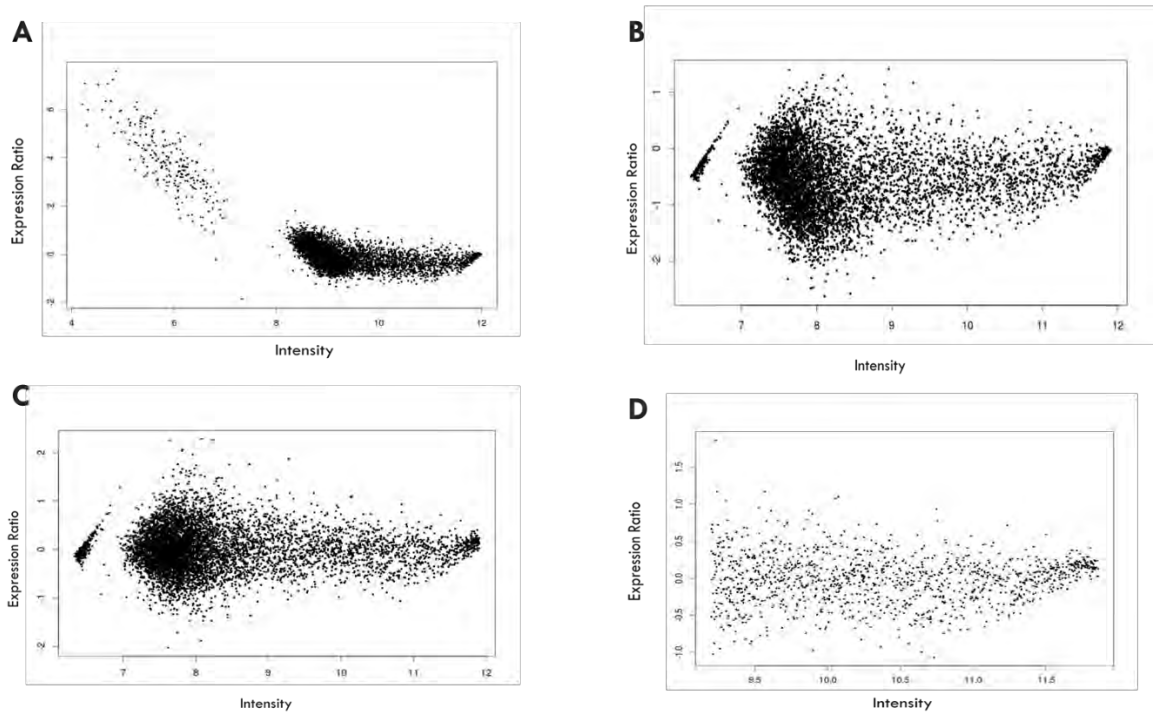


**Figure 27: Data normalization of microarray data in limma.** Data set shown has wild-type sample labeled with Cy3 and experimental sample labeled with Cy5. (A) Raw data. (B) Data following normexp background correction. (C) Data following loess normalization. (D) Data following removal of low intensity spots.

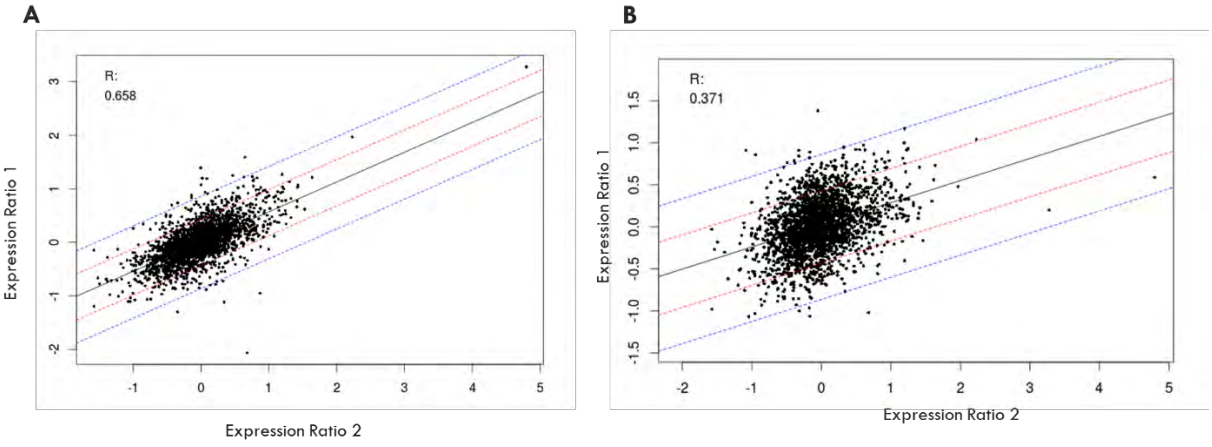


**Figure 28**: **Replicate plots of microarray data following normalization.** Data set shown has wild-type sample labeled with Cy3 and experimental sample labeled with Cy5. Line of best fit and R value included. Red dashed line indicates one standard deviation from line of best fit and blue dashed line indicates two standard deviations. (A) Replicate plot of expression ratios of within-array replicates. (B) Replicate plot of expression ratios of biological array replicates.

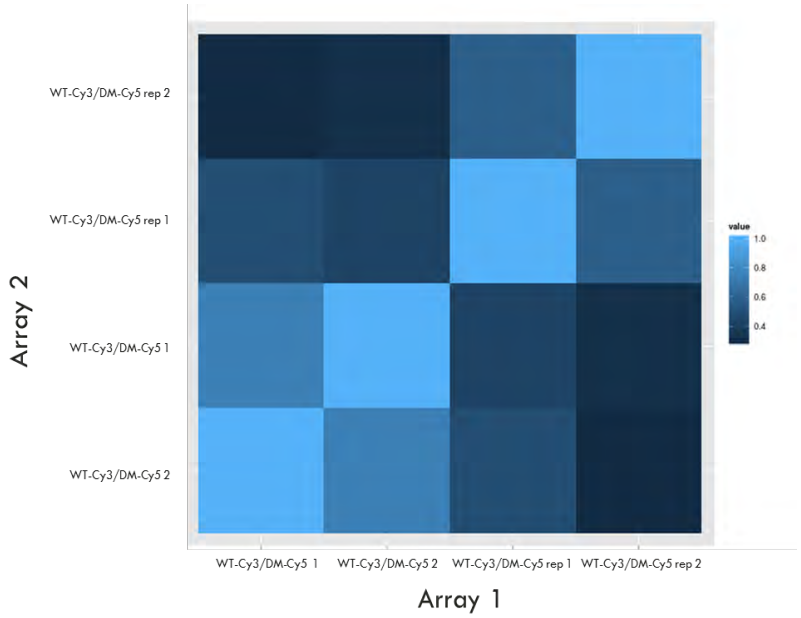


**Figure 29**: **Correlation matrix of first set of array replicates following normalization.** Data set shown has wild-type sample labeled with Cy3 and experimental sample labeled with Cy5. Pearson correlation metric used to calculate correlation between arrays. Comparison of each array against itself shown along diagonal. Upper right hand and lower left hand corners contain within-array replicate correlations. Upper left hand and lower right hand corners contain biological replicate correlations.

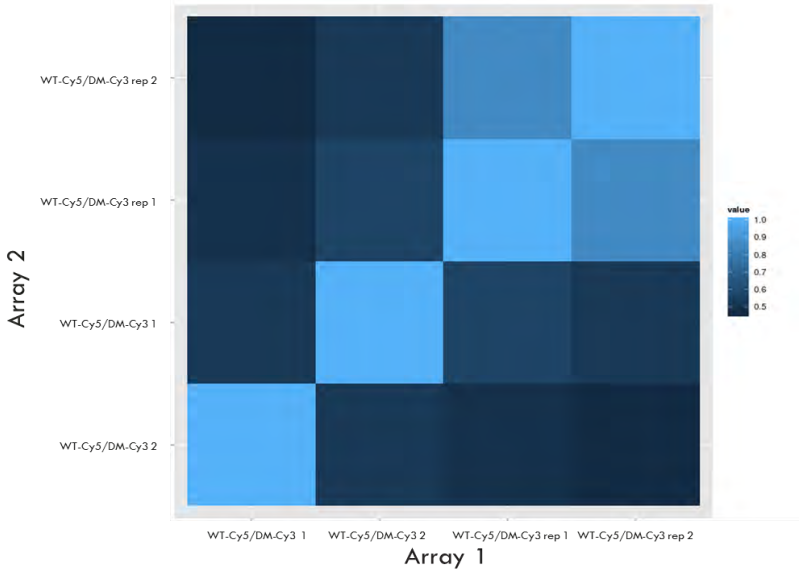


**Figure 30**: **Correlation matrix of second set of array replicates following normalization.** Data set shown has wild-type sample labeled with Cy5 and experimental sample labeled with Cy3. Pearson correlation metric used to calculate correlation between arrays. Comparison of each array against itself shown along diagonal. Upper right hand and lower left hand corners contain within-array replicate correlations. Upper left hand and lower right hand corners contain biological replicate correlations.

means clustering is a global clustering algorithm that groups observations into k groups to minimize the within-cluster sum of squares. Only genes that showed a signal above background across all four replicates were analyzed. The value of k was chosen to minimize total distance within groups while still forming large relevant clusters (Figure 31). Following k-means clustering we identified groups of genes showing consistent up- or downregulation (Figure 32). Genes belonging these groups were analyzed using the Saccharomyces Genome Database (SGD) GO Term Finder. Genes mapping to a GO term with an associated p-value of less than 0.10 based on the set of microarray background genes are highlighted (Figure 33). We observed wide-scale upregulation of carbohydrate metabolism genes and genes that respond to DNA replication stress (Figure 33A, C). Among genes showing consistent downregulation, we observed significant repression of genes responsible for ribosome biogenesis and translation (Figure 33B, D). Notably however, translation elongation factors TEF1 and TEF2 were among upregulated genes. These changes seem to suggest an overall shift towards increased energy production and decreased devotion of energy towards protein production. One possible explanation for this trend is that rRNA mutations that trigger NRD may also activate signals that warrant conservation of resources. This hypothesis may be further supported by links between NRD and ribophagy, a nitrogen starvation response which could also motivate decreased translation to conserve cellular resources.

We also reanalyzed known genes implicated in NRD and genes identified during the previous microarray experiment (Figure 34). Many of these genes did not have any spot with signal above background that made it through pre-processing. Of those that did, we saw opposite trends between the two sets of dye-swapped arrays, representative of the disagreement between dye swapped replicates that we were not able to correct during normalization.

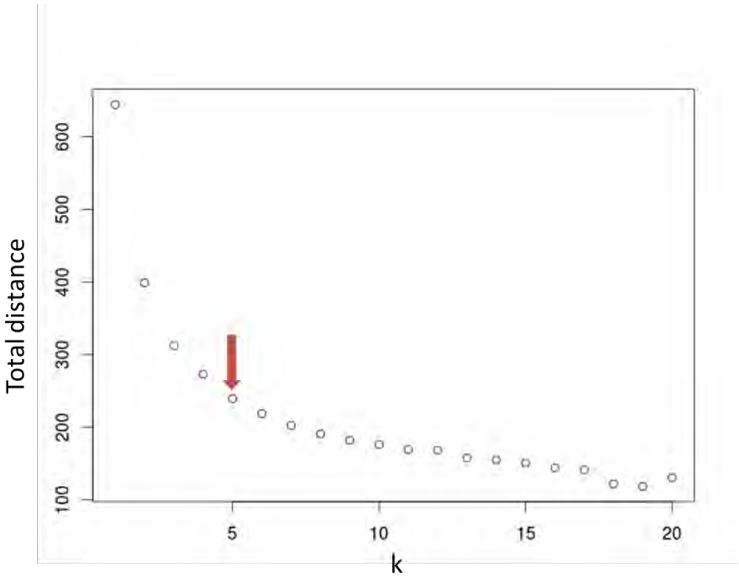


**Figure 31: Optimization of k-means clustering.** To determine the optimum k-value, where k is the number of clusters the data is divided into during k-means clustering, total distance within k groups was analyzed as a function of k. The total distance is a measure of the within-cluster sum of squares, where the sum of squares is the squared Euclidean distance. Based on this analysis, a k-value of 5 for the first data set was chosen, and a k-value of 3 for the second data set (data not shown).

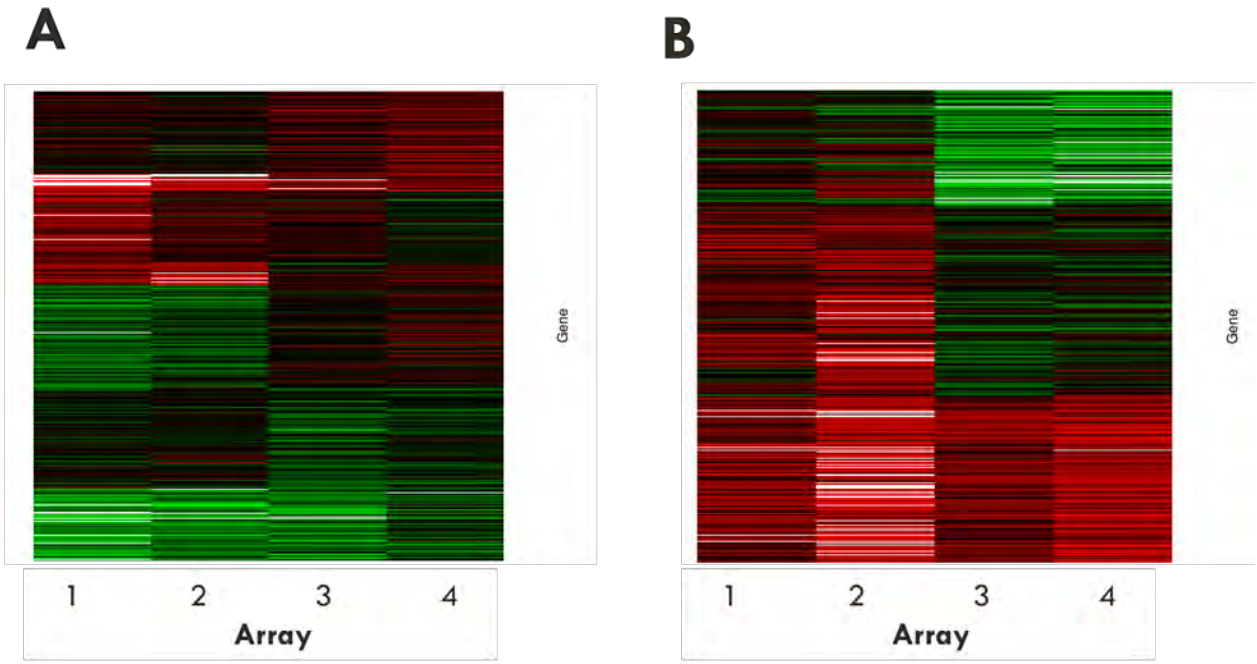


**Figure 32: k-means cluster analysis of gene expression changes observed by microarray analysis.** (A) k-means cluster analysis of within-array replicates (columns 1,2 and 3,4) and biological replicates (columns 1,3 and 2,4) for arrays with wild-type cDNA labeled with Cy3 and experimental cDNA labeled with Cy5. Arrays were normalized by normexp background correction, loess normalization and between array quantile normalization. (B) k-means cluster analysis of within-array replicates (columns 1,2 and 3,4) and biological replicates (columns 1,3 and 2,4) for arrays with wild-type cDNA labeled with Cy5 and experimental cDNA labeled with Cy3. Arrays were normalized by global median normalization and between array quantile normalization.

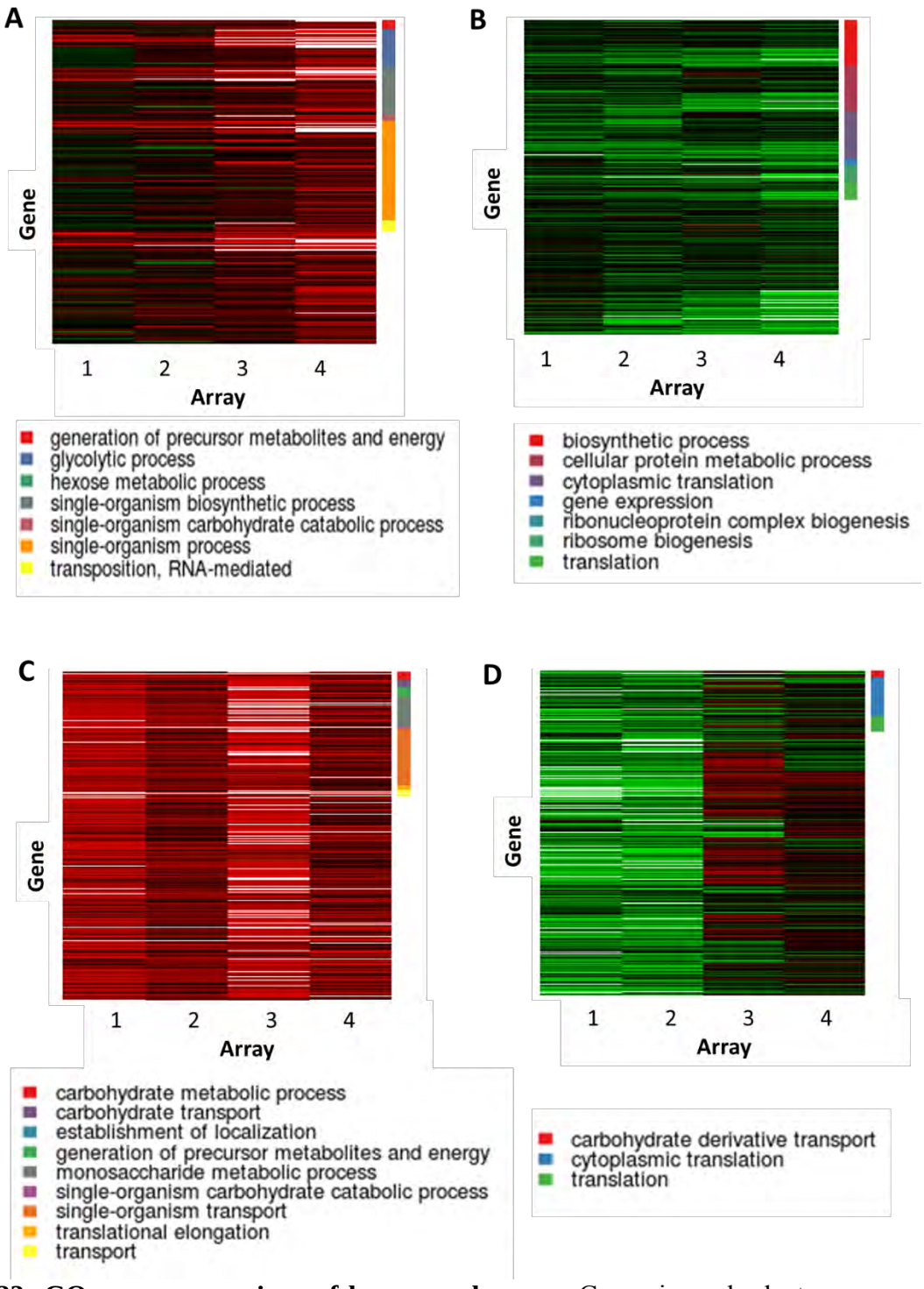


**Figure 33: GO term annotations of k-means clusters.** Genes in each cluster were analyzed using the SGD GO Term Finder. Genes mapping to GO terms with an associated p-value of less than 0.10 based on comparison with microarray background are highlighted. (A) GO term annotation of upregulated genes from Figure 32A. (B) GO term annotation of downregulated genes from Figure 32A. (C) GO term annotation of upregulated genes from Figure 32B. (B) GO term annotation of downregulated genes from Figure 32B.

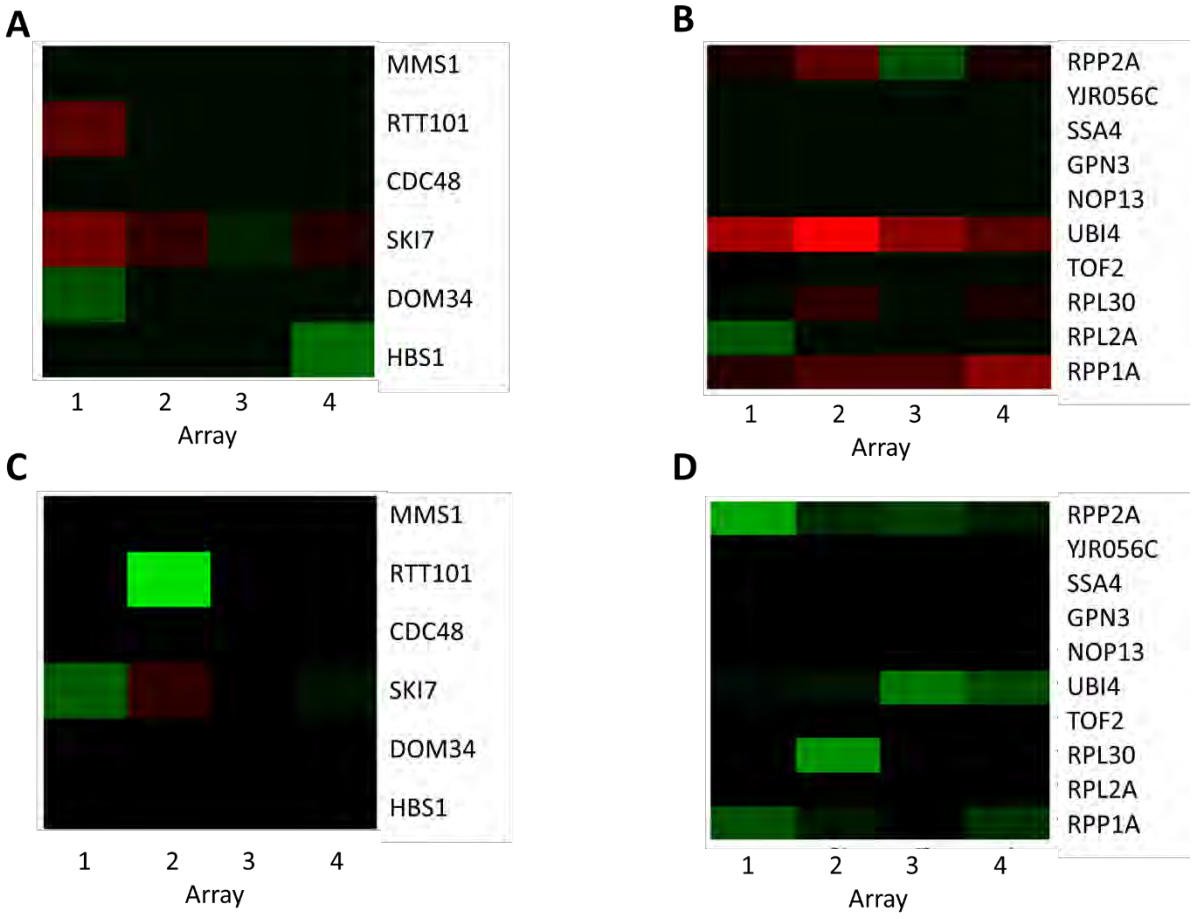


**Figure 34: Analysis of known genes and previously identified genes.** Missing values shown in black. Red corresponds to upregulated genes and green to downregulated genes. (A) Analysis of known genes from arrays with wild-type sample labeled with Cy3 and experimental sample labeled with Cy5. (B) Analysis of previously identified genes from arrays with wild-type sample labeled with Cy3 and experimental sample labeled with Cy5. (C) Analysis of known genes from arrays with wild-type sample labeled with Cy5 and experimental sample labeled with Cy3. (D) Analysis of previously identified genes from arrays with wild-type sample labeled with Cy5 and experimental sample labeled with Cy3.

We identified specific genes of interest using Differential Expression via Distance Summary for Microarray Data (DEDS) (Xiao and Yang, 2007). DEDS is a bioconductor package that combines *t* statistics (modified Student's *t*-test), *FC* (fold change), and SAM statistics (Significance Analysis of Microarrays) and selects differentially expressed genes by integrating these statistics using a weighted distance approach. Specific genes that show upregulation in response to NRD activation include TDH1, which encodes for metabolic protein GAPDH. This gene showed upregulation across both sets of arrays. In both dye-swap experiments, RNase MRP and RNase P subunit protein Pop6 also showed increased expression. While these RNases are usually involved in nuclear RNA turnover, Pop6 relocalizes to the cytosol in response to hypoxia. We also observed upregulation of RRS1, a gene which encodes for a ribosome binding protein required for nuclear export of 60S ribosomal subunits that localizes at foci along nuclear periphery. Previous FISH localization experiments have also mapped 25S NRD substrates to perinuclear foci. Another gene of notice that was downregulated is JIP5, which encodes a protein involved in biogenesis of the large ribosomal subunit that interacts with proteins involved in RNA processing, ribosome biogenesis and ubiquitination.

Additional analysis of microarray data revealed a trend across both sets of arrays of upregulation of metabolic genes and downregulation of genes involved in translation and ribosome synthesis, despite large differences between these two sets of dye-swapped arrays. Fitting these observations into the NRD framework will require additional experiments. We were also able to identify a smaller set of genes showing differential expression across arrays that may be candidates for further testing in knockout studies.

**Table 10: Partial list of differentially expressed genes identified by DEDS.[iii]**

| Gene Name | Description |
|---|---|
| TDH1 | Glyceraldehyde-3-phosphate dehydrogenase (GAPDH); involved in glycolysis and gluconeogenesis; tetramer that catalyzes the reaction of glyceraldehyde-3-phosphate to 1,3 bis-phosphoglycerate; protein abundance increases in response to DNA replication stress |
| TEF1 | Translational elongation factor EF-1 alpha; also encoded by TEF2; functions in the binding reaction of aminoacyl-tRNA (AA-tRNA) to ribosomes; may also have a role in tRNA re-export from the nucleus |
| POP6 | Subunit of both RNase MRP and nuclear RNase P; RNase MRP cleaves pre-rRNA, while nuclear RNase P cleaves tRNA precursors to generate mature 5' ends and facilitates turnover of nuclear RNAs; relocalizes to the cytosol in response to hypoxia |
| RRS1 | Essential protein that binds ribosomal protein L11; required for nuclear export of the 60S pre-ribosomal subunit during ribosome biogenesis; localizes to the nucleolus and in foci along nuclear periphery; mouse homolog shows altered expression in Huntington's disease model mice |
| JIP5 | Protein required for biogenesis of the large ribosomal subunit; required for biogenesis of the large ribosomal subunit; interacts with proteins involved in RNA processing, ribosome biogenesis, ubiquitination and demethylation; similar to WDR55, a human WD repeat protein; essential gene |

[iii]Red shading indicates increased expression, green decreased expression in response to NRD. Gene descriptions from SGD website.

## References

5 PRIME Manual Phase Lock Gel™ (PLG).
http://www.funakoshi.co.jp/data/datasheet/FPR/PLG.pdf (accessed April 2014).

Beare, R. (2007). Spot: cDNA Microarray Image Analysis Users Guide.

Bylesjö, M., Sjödin, A., Eriksson, D., Antti, H., Moritz, T., Jansson, S., and Trygg, J. (2006). MASQOT-GUI: Spot quality assessment for the two-channel microarray platform. Bioinformatics *22*, 2554–2555.

Chen, L., Muhlrad, D., Hauryliuk, V., Cheng, Z., Lim, M.K., Shyp, V., Parker, R., and Song, H. (2010). Structure of the Dom34-Hbs1 complex and implications for no-go decay. Nat. Struct. Mol. Biol. *17*, 1233–1240.

Cole, S.E., LaRiviere, F.J., Merrikh, C.N., and Moore, M.J. (2009). A Convergence of rRNA and mRNA Quality Control Pathways Revealed by Mechanistic Analysis of Nonfunctional rRNA Decay. Mol. Cell *34*, 440–450.

Van Den Elzen, A.M.G., Henri, J., Lazar, N., Gas, M.E., Durand, D., Lacroute, F., Nicaise, M., Van Tilbeurgh, H., Séraphin, B., and Graille, M. (2010). Dissection of Dom34gHbs1 reveals independent functions in two RNA quality control pathways. Nat. Struct. Mol. Biol. *17*, 1446–1452.

Dever, T.E., and Green, R. (2012). The elongation, termination, and recycling phases of translation in eukaryotes. Cold Spring Harb. Perspect. Biol. *4*.

Ding, Q., Markesbery, W.R., Cecarini, V., and Keller, J.N. (2006). Decreased RNA, and increased RNA oxidation, in ribosomes from early Alzheimer's disease. Neurochem. Res. *31*, 705–710.

Doma, M.K., and Parker, R. (2006). Endonucleolytic cleavage of eukaryotic mRNAs with stalls in translation elongation. Nature *440*, 561–564.

Doma, M.K., and Parker, R. (2007). RNA Quality Control in Eukaryotes. Cell *131*, 660–668.

Fare, T.L., Coffey, E.M., Dai, H., He, Y.D., Kessler, D.A., Kilian, K.A., Koch, J.E., LeProustt, E., Marton, M.J., Meyer, M.R., et al. (2003). Effects of atmospheric ozone on microarray data quality. Anal. Chem. *75*, 4672–4675.

Fatica, A., Oeffinger, M., Dlakiç, M., and Tollervey, D. (2003). Nob1p is required for cleavage of the 3′ end of 18S rRNA. Mol. Cell. Biol. *23*, 1798–1807.

Fromont-Racine, M., Senger, B., Saveanu, C., and Fasiolo, F. (2003). Ribosome assembly in eukaryotes. Gene *313*, 17–42.

Fujii, K., Kitabatake, M., Sakata, T., Miyata, A., and Ohno, M. (2009). A role for ubiquitin in the clearance of nonfunctional rRNAs. Genes Dev. *23*, 963–974.

Fujii, K., Kitabatake, M., Sakata, T., and Ohno, M. (2012). 40S subunit dissociation and proteasome-dependent RNA degradation in nonfunctional 25S rRNA decay. EMBO J. *31*, 2579–2589.

Genisphere Array 50$^{TM}$ Expression Array Detection Kit Protocol. http://genisphere.com/sites/default/files/pdf/Array50%20June2013.pdf (accessed April 2014).

Gentleman, R. (2005). Bioinformatics and Computational Biology Solutions Using R and Bioconductor (New York, NY: Springer Science+Business Media, Inc.).

Heyer, L.J., Moskowitz, D.Z., Abele, J.A., Karnik, P., Choi, D., Campbell, A.M., Oldham, E.E., and Akin, B.K. (2005). MAGIC Tool: Integrated microarray data analysis. Bioinformatics *21*, 2114–2115.

Ho, J.H.-N., and Johnson, A.W. (1999). NMD3 encodes an essential cytoplasmic protein required for stable 60S ribosomal subunits in Saccharomyces cerevisiae. Mol. Cell. Biol. *19*, 2389–2399.

Ho, J.H.-N., Kallstrom, G., and Johnson, A.W. (2000). Nmd3p is a Crm1p-dependent adapter protein for nuclear export of the large ribosomal subunit. J. Cell Biol. *151*, 1057–1066.

Houseley, J., LaCava, J., and Tollervey, D. (2006). RNA-quality control by the exosome. Nat. Rev. Mol. Cell Biol. *7*, 529–539.

Inada, M., and Pleiss, J.A. (2010). Chapter 3 - Genome-Wide Approaches to Monitor Pre-mRNA Splicing. In Methods in Enzymology, Jonathan Weissman; Christine Guthrie and Gerald R. Fink, ed. (Academic Press), pp. 51–75.

Jackson, R.J., Hellen, C.U.T., and Pestova, T.V. (2010). The mechanism of eukaryotic translation initiation and principles of its regulation. Nat. Rev. Mol. Cell Biol. *11*, 113–127.

Lafontaine, D.L.J. (2010). A “garbage can” for ribosomes: how eukaryotes degrade their ribosomes. Trends Biochem. Sci. *35*, 267–277.

Lafontaine, D.L.J., Preiss, T., and Tollervey, D. (1998). Yeast 18S rRNA dimethylase Dim1p: A quality control mechanism in ribosome synthesis? Mol. Cell. Biol. *18*, 2360–2370.

LaRiviere, F.J., Cole, S.E., Ferullo, D.J., and Moore, M.J. (2006). A late-acting quality control process for mature eukaryotic rRNAs. Mol. Cell *24*, 619–626.

Lee, D. (2011). Monitoring global gene expression changes in response to nonfunctional rRNA decay in Saccharomyces cerevisiae. Washington and Lee University.

Liang, W.-Q., Clark, J.A., and Fournier, M.J. (1997). The rRNA-processing function of the yeast U14 small nucleolar RNA can be rescued by a conserved RNA helicase-like protein. Mol. Cell. Biol. *17*, 4124–4132.

Nogi, Y., Yano, R., Dodd, J., Carles, C., and Nomura, M. (1993). Gene RRN4 in Saccharomyces cerevisiae encodes the A12.2 subunit of RNA polymerase I and is essential only at high temperatures. Mol. Cell. Biol. *13*, 114–122.

Powers, T., and Noller, H.F. (1990). Dominant lethal mutations in a conserved loop in 16S rRNA. Proc. Natl. Acad. Sci. U. S. A. *87*, 1042–1046.

Ritchie, M.E., Silver, J., Oshlack, A., Holmes, M., Diyagama, D., Holloway, A., and Smyth, G.K. (2007). A comparison of background correction methods for two-colour microarrays. Bioinformatics *23*, 2700–2707.

Ben-Shem, A., Jenner, L., Yusupova, G., and Yusupov, M. (2010). Crystal structure of the eukaryotic ribosome. Science *330*, 1203–1209.

Smyth, G.K. (2005). Limma: linear models for microarray data (New York).

Thompson, J., Kim, D.F., O'Connor, M., Lieberman, K.R., Bayfield, M.A., Gregory, S.T., Green, R., Noller, H.F., and Dahlberg, A.E. (2001). Analysis of mutations at residues A2451 and G2447 of 23S rRNA in the peptidyltransferase active site of the 50S ribosomal subunit. Proc. Natl. Acad. Sci. U. S. A. *98*, 9002–9007.

Vanrobays, E., Gélugne, J.-P., Caizergues-Ferrer, M., and Lafontaine, D.L.J. (2004). Dim2p, a KH-domain protein required for small ribosomal subunit synthesis. RNA *10*, 645–656.

Venema, J., and Tollervey, D. (1999). Ribosome synthesis in Saccharomyces cerevisiae. Annu Rev Genet *33*, 261–311.

Warner, J.R. (1999). The economics of ribosome biosynthesis in yeast. Trends Biochem. Sci. *24*, 437–440.

Whitworth, G.B. An Introduction to Microarray Data Analysis and Visualization. In *Methods in Enzymology*; Jonathan Weissman; Christine Guthrie and Gerald R. Fink, Eds.; Academic Press, 2010; Vol. 470, pp. 19–50.

Xiao, Y., and Yang, J.Y.H. (2007). DEDS: Differential Expression via Distance Summary for Microarray Data.

Yang, Y.H. (2009). marray: Exploratory analysis for two-color spotted microarray data.